



UIT

THE ARCTIC
UNIVERSITY
OF NORWAY

Department of Geoscience

**A combined 3D seismic and sedimentological study of the Lower
Cretaceous succession in the northeastern part of the Nordkapp Basin**

Adam Alfred Brennhaugen

Master's Thesis in Geology GEO-3900 - May 2018



Abstract

In this master's thesis in geology, 3D seismic data and shallow stratigraphic cores were used to investigate the Lower Cretaceous succession in the central sub-basin of the Nordkapp Basin, Barents Shelf.

The Lower Cretaceous is listed as a potential petroleum play model on the Barents Shelf, which makes the succession of interest for petroleum exploration. Recent studies of the have divided the Lower Cretaceous succession into seven genetic sequences, bounded by flooding surfaces. Out of these sequences, three were identified in the central sub-basin of the Nordkapp Basin. Salt diapirs are prominent in the Nordkapp Basin, including the study area, which affect the surrounding successions and are a challenge for seismic interpretation.

The two 3D seismic surveys used were ST0624 and ST0811, which cover approximately 770 km² and 1065 km² respectively in the central Nordkapp Basin. Three shallow stratigraphic cores were used for sedimentological interpretation of the Lower Cretaceous succession: 7231/01-U-01, 7231/04-U-01 and 7230/05-U-09. The cores were taken in the vicinity of the seismic survey area.

The Lower Cretaceous succession in the study area was divided into three sequences (S1–S3) based on seismic data interpretation, and correlation to other studies. An Upper Jurassic sequence was also interpreted (JS1), correlated to the Hekkingen Formation source rock. Depositional environments of the sequences were investigated in the shallow stratigraphic cores, and correlated to the seismic data. Time-thickness maps were generated to interpret the depocenters of each sequence, and their relation to each other.

Seven salt diapirs were interpreted in the study area. Based on thinning towards the diapirs in sequences JS1 and S1, the diapirs are suggested to have been active during deposition of these sequences.

A regression trend was found in the Lower Cretaceous sequences in the cores, progressing from an outer marine to inner shelf and shoreface setting. This correlates well to the sequences observed in the seismic data, where the depocenters of each sequence migrates from the NE of the study area (S1), to the middle of the study area (S2), to SW of the study area (S3). Paleogeographic maps of the study area during the deposition of the Lower Cretaceous succession, were generated.

Acknowledgement

This research is funded by ARCEX partners and the Research Council of Norway (grant number 228107).

Jeg vil bruke anledningen til å takke mine veiledere førsteamanuensis Sten-Andreas Grundvåg (UiT), universitetslektor Iver Martens (UiT) og Rune Mattingsdal (NPD) for å ha gitt meg muligheten til å skrive denne oppgaven. God dialog og tilbakemelding gjennom hele arbeidet har vært svært viktig for meg. Muligheten til å reise til Trondheim og Harstad i løpet av masterarbeidet er også satt pris på.

En takk til Atle Mørk (NTNU) ved Dora i Trondheim for en varm velkomst under loggingen av kjernene brukt i oppgaven.

En takk til mine medstudenter for samholdet gjennom masterarbeidet, for gode samtaler i lunch-pauser, og gjensidig hjelp. En ekstra takk til Thea for å ha lært meg bruk av Corel Draw, og Johanne, Stine og Hanne-Lise for en introduksjon i bruk av Petrel.

En takk til min familie for hjelp med retting av oppgaven min, og for alltid å være der for meg.

Adam Alfred Brennhaugen

Tromsø, Mai 2018

Contents

Abstract	II
Acknowledgement.....	IV
1 Introduction	1
1.1 Objectives	1
1.2 Seismic theory	3
1.3 Salt Theory	5
2 Study area and geological background.....	11
2.1 Tectonostratigraphic development of the western Barents Shelf	11
2.2 The Nordkapp Basin.....	19
3 Data and methods	25
3.1 Seismic data.....	25
3.2 Salt interpretation	30
3.3 Cores.....	31
4 Results and findings	35
4.1 Salt.....	35
4.2 Reflectors.....	39
4.3 Seismic Sequences.....	43
5 Discussion	57
5.1 Salt.....	57
5.2 Lower Cretaceous Sequences	60
5.3 Implications for paleogeographic development	65
6 Summary and conclusion	69
References	71
Appendix 1 Log of core 7230/05-U-09.....	77

1 Introduction

This chapter focuses on the understanding of prograding sedimentary successions in marine environment. During the results and discussion chapters later, this will become relevant to understand paleogeography and basin development during the Lower Cretaceous in the Nordkapp Basin area.

This study combines 3D seismic data and shallow stratigraphic cores, and aims at giving insight into the Lower Cretaceous stratigraphy of the central sub-basin in the northeastern part of the Nordkapp Basin, Norwegian Barents Shelf. The seismic data are used amongst others to interpret sedimentary sequences, salt diapirs, faults, depocenter migration, whereas the cores give direct insight into what the subsurface actually consists of. The combination of the methods therefore result in a more accurate description and interpretation of the Lower Cretaceous stratigraphy and geological history.

1.1 Objectives

The Lower Cretaceous has been listed as a potential hydrocarbon play models on the Barents Shelf (NPD, 2016), following several technical discoveries in deep to shallow marine clastic wedges. However, the paleogeography and basin development of the Barents Shelf during this time is not yet fully understood. This master's thesis will focus on identifying and characterizing several prograding sequences reported in recent studies, that span the investigation area in the central sub-basin of the Nordkapp Basin (Figure 1.1) (Marin et al., 2017; Grundvåg et al., 2017; Dimitriou, 2014). The prograding sequences will further be related to the depositional history and basin fill development of the Nordkapp Basin during the Early Cretaceous.

The Lower Cretaceous succession of the Barents Shelf was divided into seven genetic sequences (S0–S6) divided by flooding surfaces, by Marin *et al.* (2017). Three of these (S1–S3) were described in the central sub-basin of the Nordkapp Basin.

Salt domes and diapirs are prominent features in the Nordkapp Basin, and it has been suggested that they were topographic highs already in the Early Cretaceous. Therefore the identification of potential sand prone clastic wedges prograding off these salt domes is a secondary objective of this thesis.

Introduction

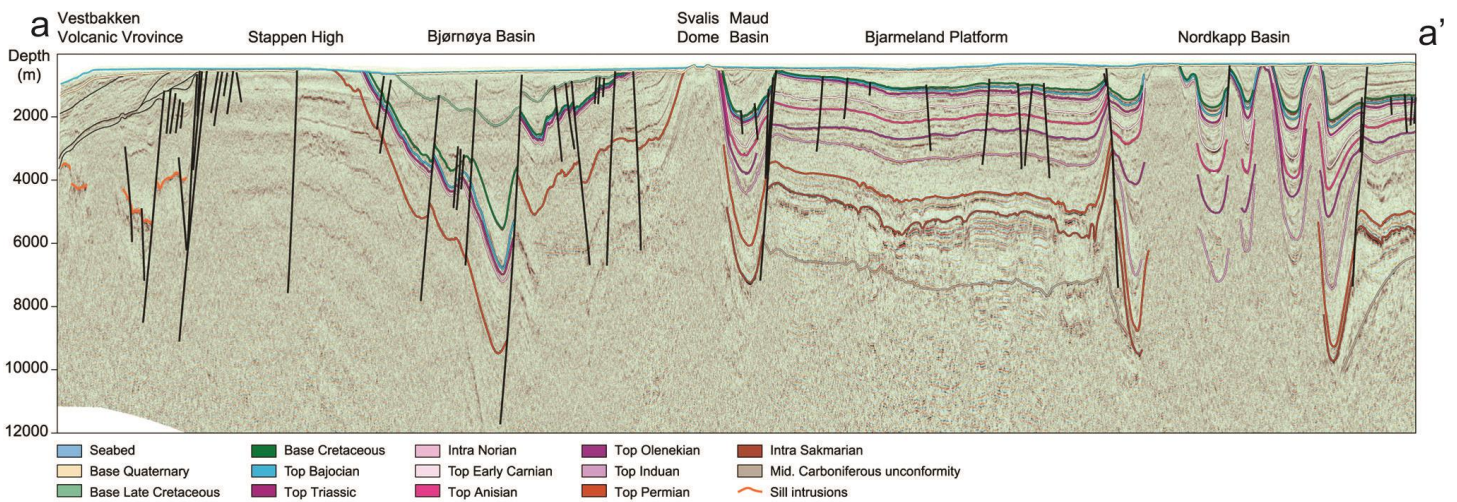
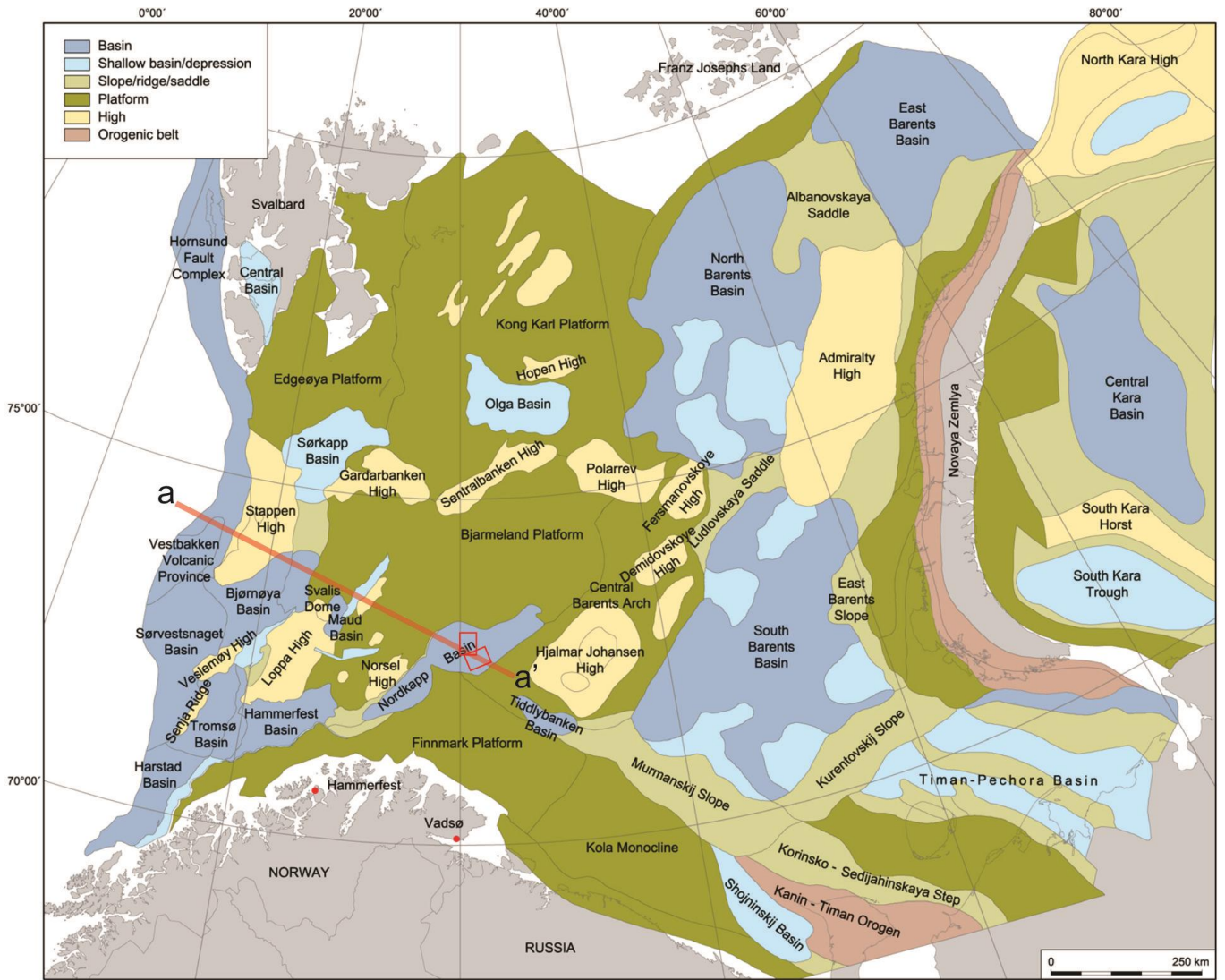


Figure 1.1. Map of structural elements on the western Barents Shelf. This study focuses on the Nordkapp Basin. The approximate study area is highlighted in red rectangles. The location seismic line a-a' is marked on the map. Modified from Henriksen et al. (2011)

1.2 Seismic theory

1.2.1 Basic reflection seismic theory

Reflection seismic is a method of mapping the subsurface by producing seismic waves and recording them as they reflect back to the surface. Seismic waves penetrating the subsurface will partially reflect surfaces where there is a change in acoustic impedance (Equation 3.1), for example between two layers of sedimentary rocks of different composition (e.g. shale overlying sandstone). Visualized horizons produced of reflected seismic waves are called reflectors.

$$Z = \rho V \quad (3.1)$$

Equation 3.1: The acoustic impedance of a seismic layer, Z , is its density (ρ , kg/m^3) multiplied by its acoustic velocity (V , m/s).

The amount of energy reflected when the seismic wave hits a reflector, is determined by the magnitude of change in acoustic impedance at the boundary, and is described by the reflection coefficient (Equation 3.2). The reflected energy is measured back on the surface by measuring equipment, like a hydrophone cable for surveys at sea (Andreassen, 2009).

$$R = \frac{(Z_2 - Z_1)}{(Z_2 + Z_1)} = \frac{(\rho_2 V_2 - \rho_1 V_1)}{(\rho_2 V_2 + \rho_1 V_1)} \quad (3.2)$$

Equation 3.2: The strength of the reflection generated when the seismic wave hits a contrast in acoustic impedance is quantified as the boundaries reflection coefficient (R). Z_1 , ρ_1 and V_1 are respectively the acoustic impedance, density and seismic velocity of the upper layer. Z_2 , ρ_2 and V_2 are respectively the acoustic impedance, density and seismic velocity of the lower layer. If $Z_1 = Z_2$, no reflection is generated.

The reflection coefficient can be either positive or negative, depending on if the seismic signal is traveling from a layer of lower acoustic impedance into a layer of higher acoustic impedance, or *vice versa*. If $Z_1 > Z_2$, the reflection will have a positive amplitude (peak), whereas if $Z_1 < Z_2$, the reflection will have a negative amplitude (trough), as per the European Association of Geoscientists and Engineers (EAGE) (Jackson and Hudec, 2017). The time it takes the seismic signal to reach a reflector, and travel back up to the measuring equipment, is the two-way traveltime (TWTT). If the approximate seismic velocity of the

Introduction

subsurface is known, for example from well data in the area, the TWTT can be converted to depth (Equation 3.3) (Andreassen, 2009).

$$Depth = \frac{1}{2} (TWTT * V) \quad (3.3)$$

Equation 3.3: Equation used for converting two-way traveltime (TWTT, ms) to depth (m), if the velocity (V, m/s) is known.

1.2.2 Seismic facies analysis and stratigraphy

Seismic facies analysis entails the categorization of seismic facies units within seismic sequences, based on objective seismic parameters, including reflection configuration (Figure 1.3 and Figure 1.4), continuity, amplitude, frequency and interval velocity (Mitchum Jr. et al., 1977). A seismic sequence is defined as a succession of relatively conformable reflectors, bounded by at its top and base by discontinuity surfaces (Figure 1.2) (Mitchum Jr. et al., 1977).

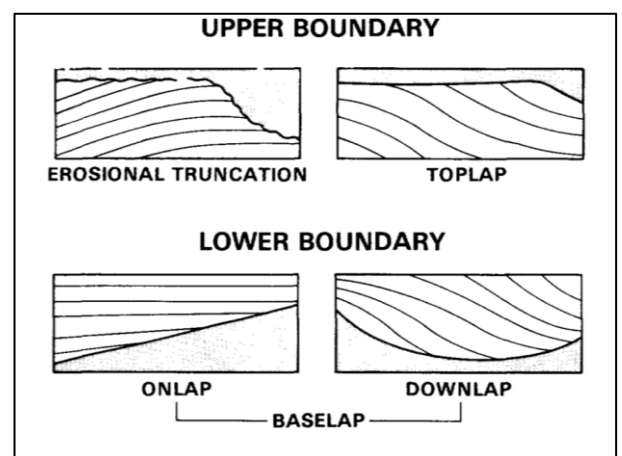


Figure 1.2 Seismic sequence upper and lower boundaries, defined by surfaces where reflectors terminate. Figure from Mitchum Jr., et al. (1977).

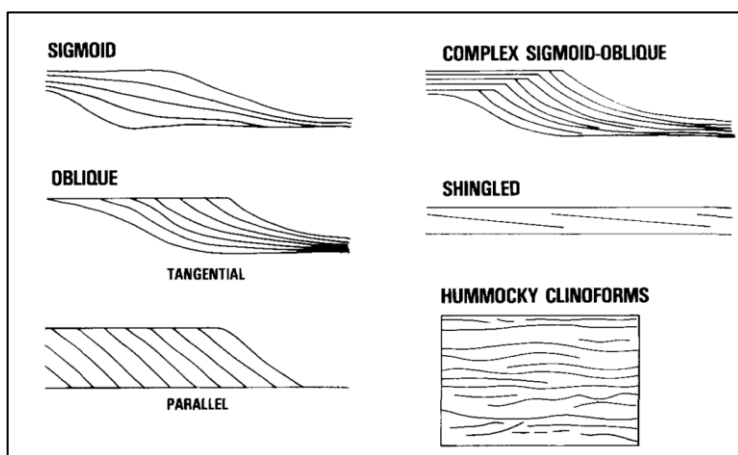


Figure 1.3 Patterns of seismic reflections interpreted as prograding clinoforms. Figure from Mitchum Jr. et al., (1977).

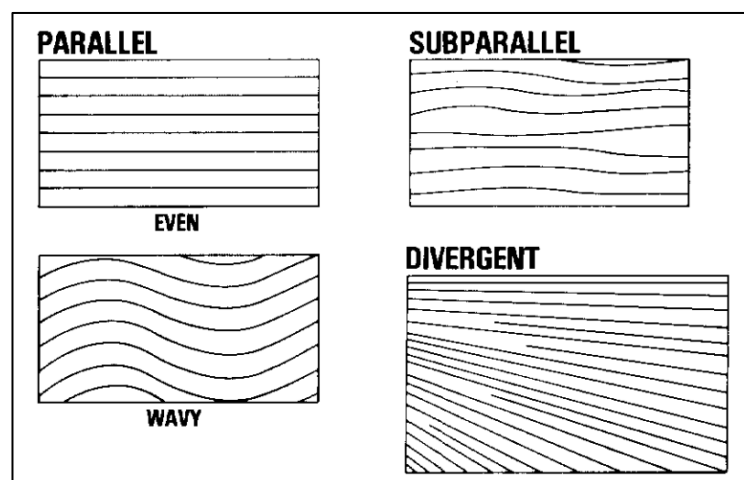


Figure 1.4 Examples of reflector configurations – parallel, subparallel and divergent. Figure from Mitchum Jr. et al., (1977).

1.3 Salt Theory

1.3.1 Salt deposition

Evaporites are minerals precipitated out of water, when the concentration of ions is increased due to evaporation (Nichols, 2009). Some of the most common evaporite minerals are gypsum ($\text{CaSO}_4 \cdot 2\text{H}_2\text{O}$), anhydrite (CaSO_4), halite (NaCl), sylvite (KCl), and the carbon bearing minerals calcite (CaCO_3) and dolomite ($\text{CaCO}_3 \cdot \text{MgCO}_3$) (Table 1). Calcium carbonates are the first minerals to precipitate from evaporating water, due to being the least soluble component. Gypsum and anhydrite follow, then halite, as the ions in the water become more concentrated. Potassium and magnesium chlorides are the last to precipitate, and require a very high ion concentration (Nichols, 2009). The composition of evaporites deposited is dependent of the water type, temperature and salinity of the depositional environment (Nichols, 2009). Variability in the depositional environment, e.g. where water level changes in an arid lagoon, may result in interbedded laminated and nodular gypsum, deposited respectively subaqueously and in a supratidal sabkha (Nichols, 2009). Interbedding by clastic or carbonate sediments is also common.

Table 1. Physical properties of common evaporate minerals. After Jones and Davison (2014).

Mineral	Composition	Hardness	Density (kg/m^3)	Seismic velocity (m/s)
Halite	NaCl	2.5	2200	4500
Gypsum	$\text{CaSO}_4 \cdot 2\text{H}_2\text{O}$	1.5–2	2300	5700
Anhydrite	CaSO_4	3.5	2900	6500
Dolomite	$\text{CaCO}_3 \cdot \text{MgCO}_3$	3.5–4	2870	6300
Sylvite	KCl	1.5–2	1990	4110

1.3.2 Salt migration and structures

The pressure required to make salt minerals act plastic, is low. Only a few hundred meters of overburden is required to make halite act plastic (Fossen, 2010). Due to the low density of the salt, compared to sandstone or limestone, the salt tends to migrate upwards, towards thinner parts or zones of weakness (ex. faults) in the overburden (Nichols, 2009). There are a multitude of different shapes that the resulting salt may take, described amongst others by Trusheim (1960) and Fossen (2010). A common collective term for salt structures that pierce overburden, driven by density contrasts, is salt diapir (Fossen, 2010), and the term will thus be used in this thesis.

Introduction

Trusheim (1960) proposed the terms salt pillows, salt stocks and salt walls, respectively increasing in size and extent (Figure 1.5A), to describe halokinetic structures in Northern Germany. He related the increase of size and extent (collectively *maturity*) of the structures to the thickness of the original salt layer in the Zechstein Basin. The central Zechstein basin, with the thickest original salt layer, would preferably develop into large salt walls (4–5 km width, up to more than 120 km length). Peripherally towards the basin flanks, the original salt layer was thinner, and salt stocks (circular, oval, elliptical or elongated outline included) and salt pillows developed (Trusheim, 1960).

Fossen (2010) describes additional halokinetic structures, divided into linear structures (salt roller, anticline, wall and canopy) and circular structures (salt pillows, stocks, glacier and sheets) (Figure 1.5B).

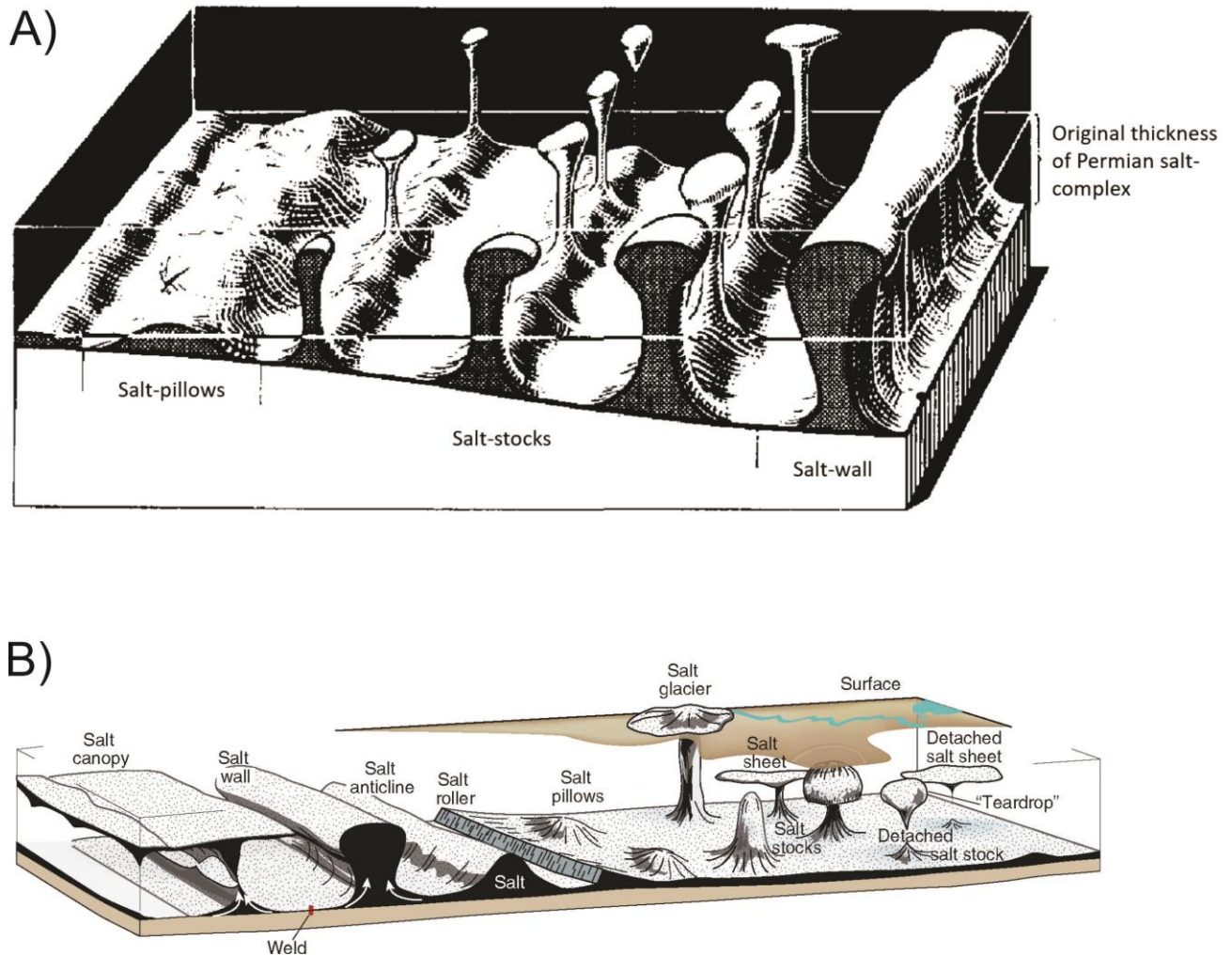


Figure 1.5. Classification of salt structures. A) Classification of salt structures, in relations to the original thickness of a Permian salt-complex, Northern Germany. Modified after Trusheim (1960). B) Classification of salt structures, maturing from the centre, with linear structures to the left, and circular structures to the right. Figure from Fossen (2010).

1.3.3 Halokinetic sequences

When salt structures pierce the overburden and grow, surrounding areas subside, as the salt layer is concentrated in the diapir (Trusheim, 1960; Giles and Rowan, 2012). The subsidence will commonly be compensated by levelling infill of sediments, as well as roof sediments sliding to the sides of the diapir during breakthrough of the overburden. This is referred to as active diapirism (Giles and Rowan, 2012; Giles and Lawton, 2002; Fossen, 2010). When a diapir rises continually at the same rate as surrounding sedimentation, the diapir is referred to as passive. Adjacent to passive diapirs, two end members of halokinetic sequences bounded by disconformities are described by Giles and Rowan (2012), based on stratal geometry. The two end members are hook and wedge halokinetic sequences, and are typically some tens of meters in thickness (Figure 1.6 a and b) (Giles and Rowan, 2012). Further, stacks of these sequences are referred to as respectively tabular and tapered composite halokinetic sequences (Figure 1.6 c and d). The packages can be hundreds of meters in total thickness.

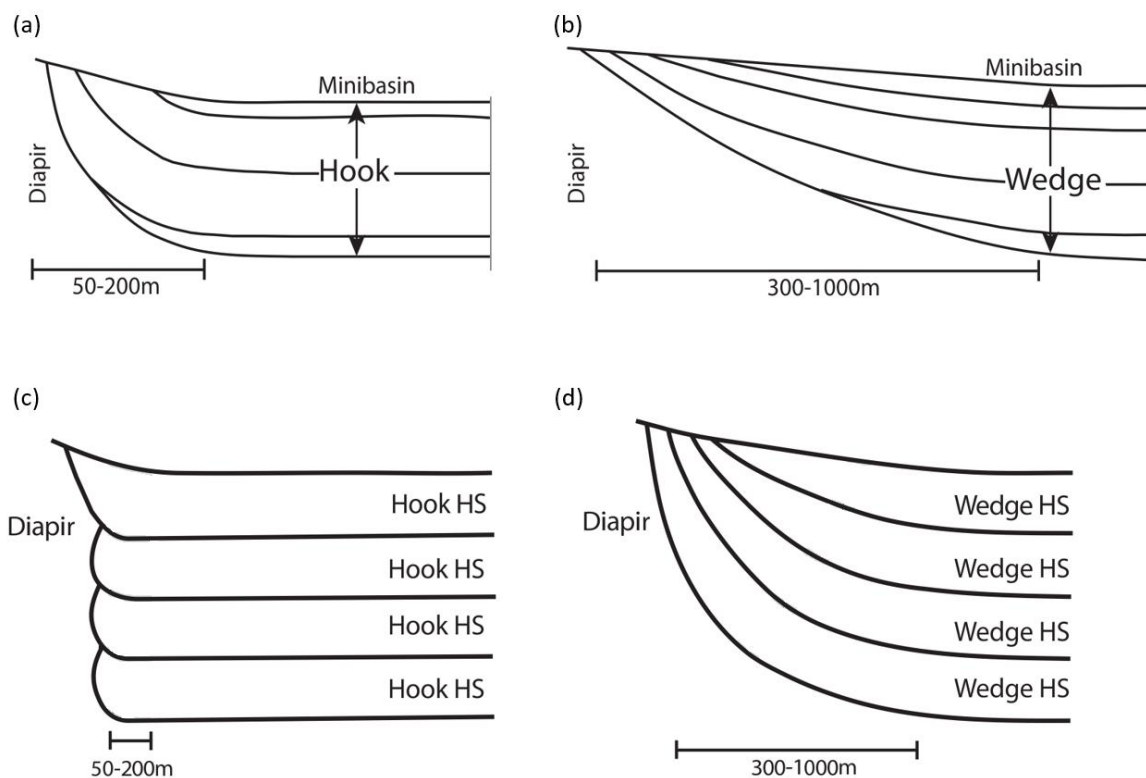


Figure 1.6. End-member model for halokinetic sequences and composite halokinetic sequences (CHS), modified after Giles and Rowan (2012): (a) Hook type halokinetic sequence. (b) Wedge type halokinetic sequence. (c) Tabular CHS. (d) Tapered CHS.

1.3.4 Challenges with interpreting salt in seismic data

The visualization and interpretation of salt in seismic data presents some challenges, mainly due to the potentially complex morphology of salt diapirs and the seismic velocity of salt compared to typical surrounding sediments (Jackson and Hudec, 2017).

Morphological challenges

Jackson and Hudec (2017) present four main challenges of salt imaging and interpretation, related to the complex morphologies of salt diapirs:

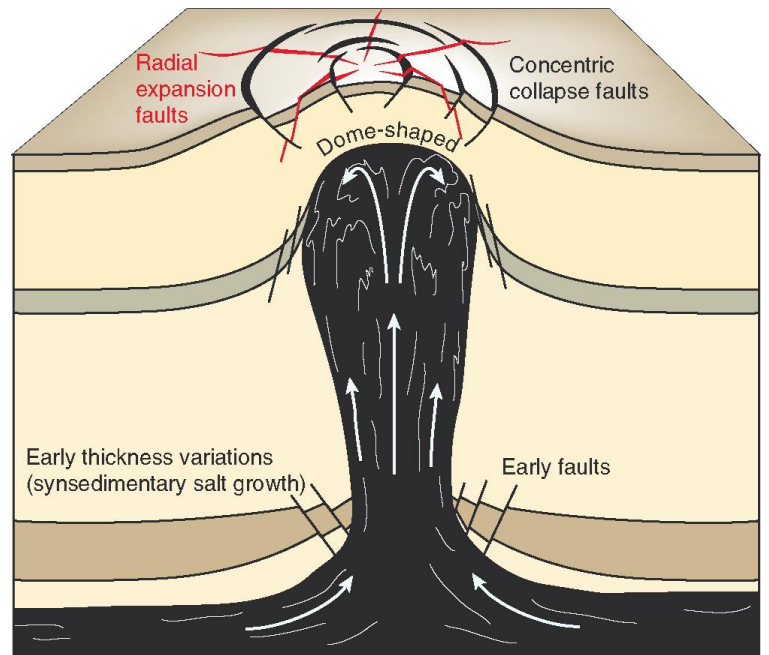


Figure 1.7. Structures formed around a salt diapir not reaching the surface. Radial expansion faults are marked in red. Figure from Fossen (2010).

- Over short distances, the form of diapirs can change drastically. As a result of this, translating interpretations of diapirs from a well-imaged to a poor-imaged area, can cause uncertainties.
- The boundary on the sides of salt diapirs is commonly a very steep interface between surrounding sediments, and the salt body. Surrounding sediments may also be bent to near vertical positions (see chapter 1.3.3 Halokinetic sequences). Steep dipping features are often poorly imaged in seismic data.
- Fault complexes are common additions to diapirs and may cause uncertainty when interpreting seismic horizons near the salt body. Salt diapirs that move, but do not reach the surface, often result in overlying sediments doming upwards, as they are pushed by the diapir from below (Figure 1.7) (Fossen, 2010). Normal faults are common in the overlying rock, either in a circular form (concentric collapse faults, or ring faults (Jackson and Hudec, 2017)), or as rays, with the fault plane's strike radiating outward from the salt body below (radial expansion faults).
- Seismic velocity anisotropy, due to modifications in stress and pore pressure in sediments surrounding salt bodies, are difficult to process, when acquiring seismic data.

Seismic velocity challenges

With the P-wave velocity in pure halite being 4500 m/s, and impure salt slightly lower, the velocity in salt bodies is generally much higher than typical water saturated shales or sandstones (1500–2200 m/s). Salt is usually impure, containing anhydrite, gypsum, sylvite, carbonates or other inclusions (see Table 1) (Jackson and Hudec, 2017; Jones and Davison, 2014). The big contrast in P-wave velocity at the interface between the salt and surrounding sediments, together with complex salt body geometries, causes a distortion in the seismic wave field (Jackson and Hudec, 2017).

One typical data distortion caused by salt bodies is velocity pull-up. When the seismic waves travel through the salt body, it may travel faster than through the surrounding sediments, making strata below the salt appear at a shallower depth than side lying sediments, in the time domain. A velocity push-down of subsalt strata is also possible, although less common, if the velocity of the overlying salt body is slower than the surrounding rock (Jackson and Hudec, 2017).

Another common distortion of data caused by salt bodies, is seismic shadow (Figure 1.8). As seismic waves arrive at a salt body surrounded by sediments, the wave is reflected both when hitting the top of the salt, and again when hitting the bottom salt-sediment contact. At both interfaces refracting waves are distorted. The potential effect of this distortion, is that some subsalt areas are left in seismic shadow, without any seismic waves passing through or returning to the seismic receivers, giving no data from the area.

(Jackson and Hudec, 2017; Jones and Davison, 2014).

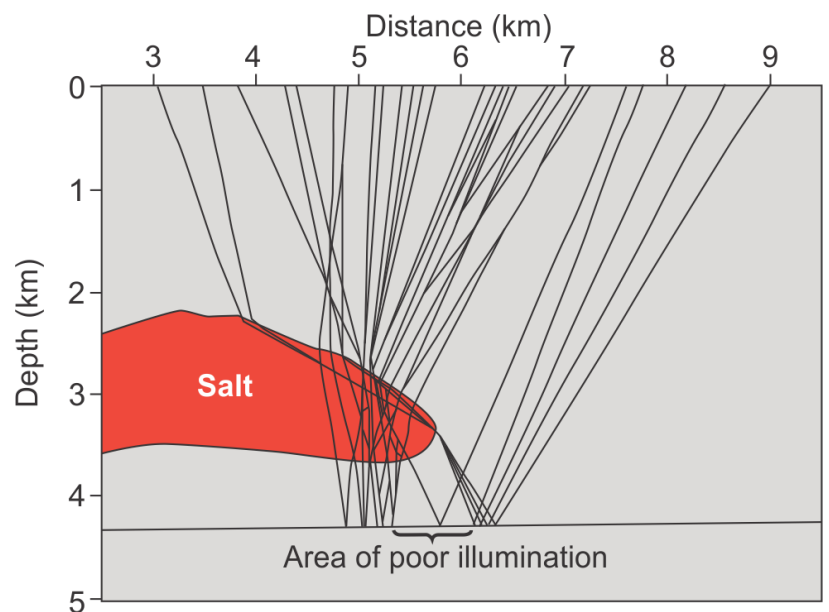


Figure 1.8. Shot-gather ray-trace diagram showing how a subsalt area may be left in shadow (poor illumination) as seismic waves are refracted through the salt body (red). Figure from Jackson and Hudec (2017).

2 Study area and geological background

The Barents Sea is a shallow shelf sea situated on the northwestern edge of the Eurasian tectonic plate. It is bounded to the west by the Norwegian-Greenland Sea, to the south by the coasts of Norway and Russia, to the east by the Novaya Zemlya archipelago, and to the north by the Svalbard and Franz Josef Land archipelagos (Figure 2.1) (Smelror et al., 2009). The Nordkapp Basin, the focus area for this study, lies in the eastern part of the western Barents Shelf (Figure 1.1).

2.1 Tectonostratigraphic development of the western Barents Shelf

The geological history of the western Barents Shelf is known to be more complex than that of the other parts of the Norwegian continental shelf (the North Sea and Norwegian Sea) (Faleide et al., 2015). The southwestern part of the Barents Shelf is dominated by a series of basins (Sørvestnaget, Hammerfest, Bjørnøya, Nordkapp basins) separated by highs (Loppa, Stappen, Norsel highs and Finnmark and Bjarmeland platforms) (Figure 1.1). These are a result of two orogenic events, three main extensional rifting phases, uplift of the Barents Shelf during the Cenozoic era, and a finishing polish by Pleistocene glaciation (Doré, 1995; Gernigon et al., 2014; Faleide et al., 1993).

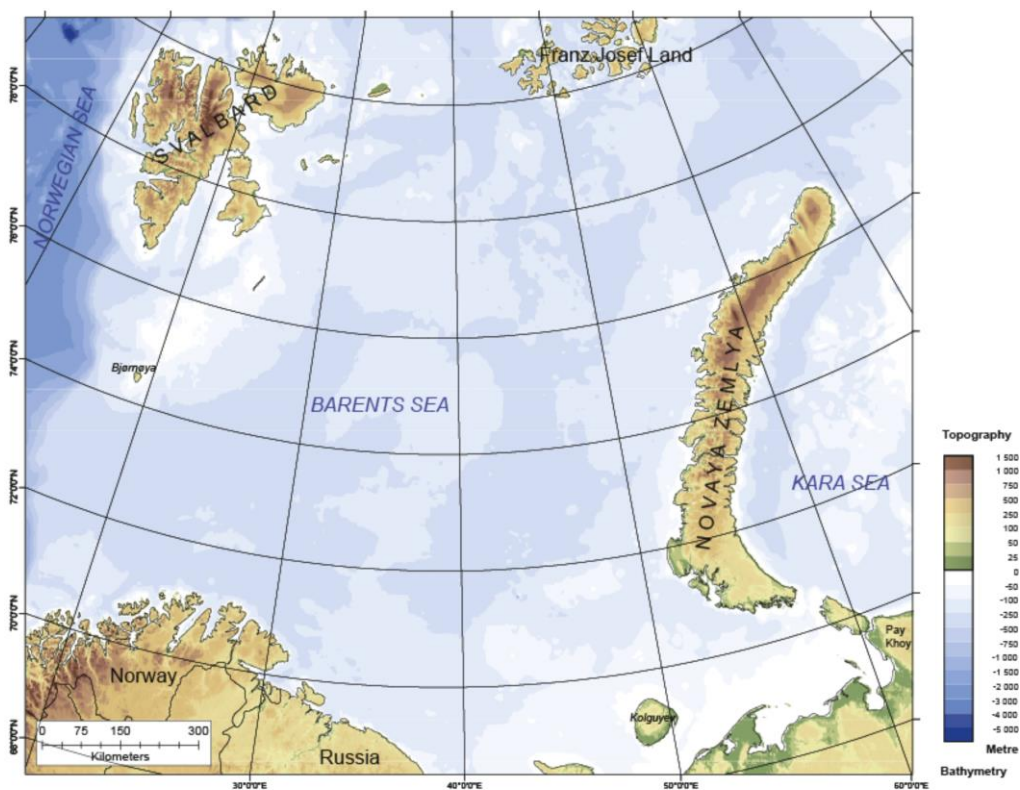


Figure 2.1 Geographical map of the Barents Sea. Figure from Smelror et al. (2009).

2.1.1 Paleozoic tectonostratigraphic development

Structural and tectonic development

Collectively, the basement of the Barents Shelf and Svalbard archipelago is referred to as Hecla Hoek, and includes both Precambrian and Cambrian to Silurian metamorphic, metasedimentary and magmatic rocks (Worsley, 2008). Compressional tectonics during the Caledonian orogeny, between the Late Silurian and Early Devonian, is the first major tectonic event that played a role in establishing the present structural setting of the Barents Shelf (Doré, 1995; Gabrielsen et al., 1990). The Caledonian orogeny resulted in the merging of the Laurentian (Greenland, North America) and Baltic (Norway) tectonic plates around 400 million years ago, closing the Iapetus Ocean, correlative in position to the northern Atlantic Ocean today (Worsley, 2008). The Caledonian orogeny, together with the later Uralian orogeny, merged most of earth's landmasses to the supercontinent Pangaea in Permian to Triassic times (Doré, 1995; Smelror et al., 2009).

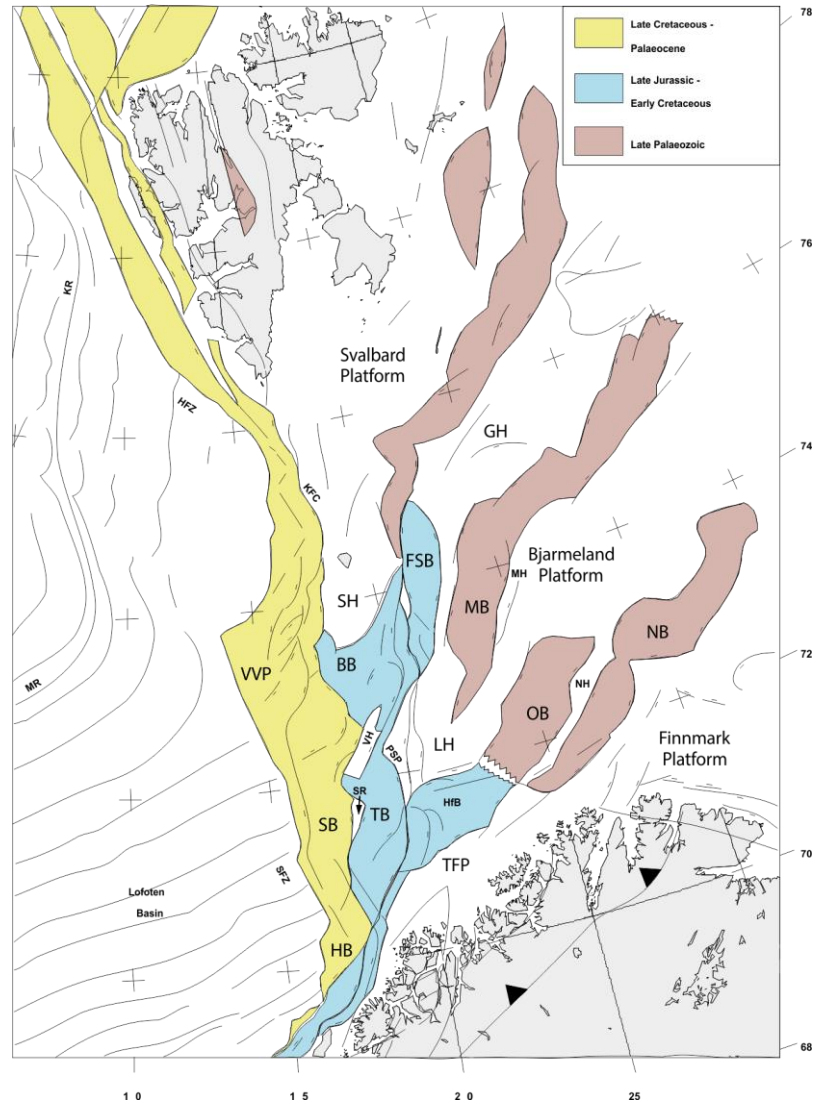


Figure 2.2 Main structural elements of the western Barents Sea. Areas are colour coded based on when they were developed. BB = Bjørnøya Basin, FSB = Fingerdjupet Sub-basin, GH = Gardarbanken High, HB = Harstad Basin, HfB = Hammerfest Basin, HFZ = Hornsund Fault Zone, KFC = Knølegga Fault Complex, KR = Knipovich Ridge, LH = Loppa High, MB = Maud Basin, MH = Mercurius High, MR = Mohns Ridge, NB = Nordkapp Basin, NH = Nordsel High, OB = Ottar Basin, PSP = Polheim Sub-platform, SB = Sørvestsnaget Basin, SFZ = Senja Fracture Zone, SH = Stappen High, SR = Senja Ridge, TB = Tromsø Basin, TFP = Troms-Finnmark Platform, VH = Veslemøy High, VVP = Vestbakken Volcanic Province. Figure from Faleide et al. (2015).

Extensional collapse in the form of rifting, following the Caledonian orogeny, from Late Devonian to middle Permian, formed several fault-bounded basins and highs on the western Barents Shelf (Faleide et al., 2015). The Tromsø, Bjørnøya, Nordkapp, Fingerdjupet, Maud and Ottar basins are all thought to have formed during these rifting events mainly during the

Study area and geological background

middle Carboniferous. Generally, tectonically induced structures, like basins, highs and fault zones, on the western Barents Shelf follow a N–S to NE–SW trend, directed by the Caledonian orogeny. On the eastern shelf a N–S lineation is most prominent, following the Uralian orogeny (Doré, 1995).

Whereas the eastern Barents Shelf saw the closure of the Uralian Ocean during the Uralian orogeny from Late Carboniferous through Permian time, the western shelf was dominated by regional extension during this time (Smelror et al., 2009).

Paleozoic stratigraphic and depositional development

Throughout the rift events in the Paleozoic, syn- and post-rift sediments filled and eventually draped the newly formed basins. Carbonate and evaporate deposition dominate the Upper Carboniferous and Lower Permian strata (Gipsdalen Group - Figure 2.3), deposited on shallow marine ramp settings during highstand, and leaving large areas exposed as sabkhas during lowstand sea level (Worsley, 2008). The salt deposited during this time reaches up to 4–5 km thickness in the Nordkapp Basin (Faleide et al., 2015), which later remobilized into diapirs. What was a warm water carbonate platform during Late Carboniferous and earliest Permian, changed to a cool and cold water carbonate platform during the middle to Late Permian (Sakmarian) (Bjarmeland Group - Figure 2.3). This was the result of the continent drift northwards on the globe, from a paleolatitude of 20°N during Carboniferous–Permian, and up towards 55°N in the Late Triassic (Ahlborn and Stemmerik, 2015).

2.1.2 Mesozoic tectonostratigraphic development

Structural and tectonic development

Rifting continued in the western Barents Shelf from Permian to Early Triassic, and subsequent post-rift subsidence took place both during Middle and Late Triassic. Between the Early Triassic and Middle Jurassic, the western Barents Shelf was relatively tectonically quiet. (Glørstad-Clark et al., 2010; Smelror et al., 2009).

Regional extension occurred in the southwestern Barents Shelf again in the Middle Jurassic to Early Cretaceous, further opening more deep basins, along with strike-slip movement along older structures (Faleide et al., 1993). Deep rift basins developed during this period include the Bjørnøya, Tromsø, Sørvestnaget and Harstad basins (Doré, 1995; Faleide et al., 1993).

During the Barremian to Aptian, volcanism was active in the northern to northeastern part of the Barents Shelf, resulting in the High Arctic Large Igneous Province (Smelror et al., 2009; Polteau et al., 2016). The uplift caused by the volcanic activity gave rise to sediment influx from the north, succeeded by southward progradation (Faleide et al., 2008). In the Late

Cretaceous, large parts of the Barents Shelf were uplifted (Smelror et al., 2009).

The Late Cretaceous is known to be a time of sediment starvation in large parts of the Barents Shelf (Worsley, 2008). The exception are basins on the southwestern shelf (e.g. the Tromsø

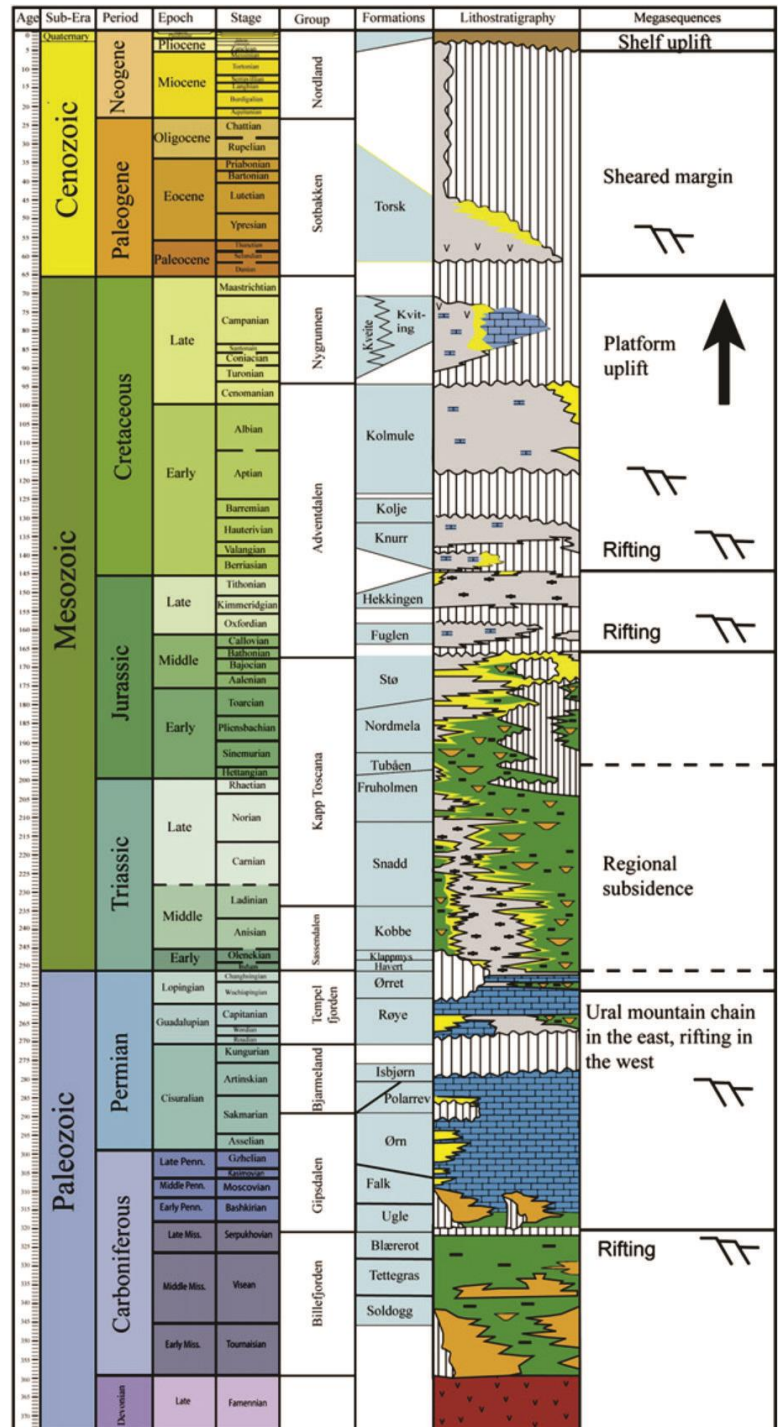


Figure 2.3 Lithostratigraphy in the western Barents Sea, with formation names and main structural events indicated. Modified from Glørstad-Clark et al. (2010).

and Sørvestnaget basins) which continued to subside due to continued extension (Faleide et al., 2015).

Mesozoic stratigraphic and depositional development

During the Triassic period, parts of the Barents Shelf saw the shift from a deep-water basin in the Early Triassic, to infills of sediments from newly formed Ural Mountains in the east. The basins were filled with deltaic successions, and some areas were subaerially exposed during the Middle Triassic (Sassendalen Group - Figure 2.3) (Faleide et al., 2015; Glørstad-Clark et al., 2010; Riis et al., 2008). Central and northern basins remained deeper marine environments until Late Triassic, as progressively basins were filled with sediments to the east in Late Permian and Early Triassic, then to the south, before prograding into the northwestern Barents Shelf during the Carnian (Glørstad-Clark et al., 2010; Lundschieen et al., 2014; Riis et al., 2008). High subsidence, and sedimentation rates are characteristic for the Triassic period until the early Norian (Worsley, 2008), when a seaway was opened between the Tethys and Boreal oceans.

Early to Middle Jurassic strata on the Barents Shelf is dominated by shallow marine and coastal deposited sandstones, as subsidence rates and sediment supply from the Uralian Highland decreased (Smelror et al., 2009). The coarser clastic sediments were cut off during the Bathonian, when a regional transgression led to finer clastic sediment deposits dominating (Adventdalen Group - Figure 2.3). It was during this time that the black shales of the Upper Jurassic Hekkingen Formation were deposited in anoxic–dysoxic conditions all across the Barents Shelf (Faleide et al., 2015; Worsley, 2008; Smelror et al., 2009).

The transition from Jurassic to Cretaceous saw a major change in depositional environment on the Barents Shelf, caused by a lowering of the sea level (Smelror et al., 2009; Worsley, 2008). Marine deposited clastic sediments still dominated basins, but condensed carbonate platforms are found from this time on structural highs (Smelror et al., 2009). The opening of the Amerasian Basin in the Arctic Ocean led to extensive magmatism in the High Arctic Large Ingenious Province, and an uplift of the northernmost Barents Shelf, during Early Cretaceous (Smelror et al., 2009; Polteau et al., 2016). This highland was the source area for large southward prograding deltaic clinoforms, depositing across the shelf, causing further regional regression and extending more near-shore and continental depositional environments (Smelror et al., 2009). On Svalbard this transition can be seen in the Lower Cretaceous Rurikfjellet Formation being dominated by marine shales, and the overlying Helvetiafjellet

Study area and geological background

Formation consisting of paralic deposits containing thin coals (Smelror et al., 2009; Grundvåg et al., 2017). Southern parts of the western Barents Shelf continued to be more open marine settings during the middle Lower Cretaceous, with shales being deposited in the basins (Smelror et al., 2009; Worsley, 2008). Around Albian a large transgressive event caused a general deepening in depositional environment in the western Barents Shelf, and many of the previous near-coast and continental environments transformed into shallow marine settings. On Svalbard, this can be seen in the Carolinefjellet Formation, where shallow marine and nearshore deposits are found overlying continental and deltaic strata of the Helvetiafjellet Formation (Smelror et al., 2009).

Strata from the Upper Cretaceous seems to be found only in the marginal basins of the western Barents Shelf, where sequences thin eastward onto structural highs (Nygrunnen Group - Figure 2.3) (Worsley, 2008). According to Worsley (2008), a 1200 m claystone of Upper Cretaceous age was found in wells in the Tromsø Basin, thinning eastward to under 250 m in the Hammerfest Basin. Uplift and erosion seem to be the cause why little to no Upper Cretaceous depositions are found in the northern parts, where Paleogene sediments discordantly overly Lower Cretaceous strata (Worsley, 2008; Smelror et al., 2009).

2.1.3 Cenozoic tectonostratigraphic development

Structural and tectonic development

Around 55–54 million years ago the opening of the northern Atlantic Ocean, the Norwegian-Greenland Sea, marks the transition from Paleocene to Eocene, and a large development of the western continental margin of the Barents Shelf (Worsley, 2008). A complex interplay between stepwise rifting and shearing along the margin occurred, between the Barents Shelf, Svalbard and Greenland. A continental strike-slip system was the main driver of movement from Paleocene to Eocene, progressing into a passive shear-margin, and finally to breaking up and the formation of oceanic crust during Eocene/Oligocene (Faleide et al., 1984).

Volcanic intrusive activity during the spreading between the two continents has also been identified, as eight tectonic events and three volcanic events within the Vestbakken Volcanic Province have been reported during the Cenozoic extensional rifting (Faleide et al., 2008).

Uplift between Late Pliocene and Pleistocene, and subsequent erosion, particularly during Pleistocene glaciation, strongly affected the areas close to the western margin. The amount of sediments uplifted and eroded during this time increase towards the north and west on the

Study area and geological background

Barents Shelf. Up to 2–3 km of sediments were removed on the platform areas around Svalbard. Further south, around 2 km of sediments are thought to have been uplifted and eroded, at the Hammerfest Basin, the Nordkapp Basins, and on the Loppa High (Smelror et al., 2009). Sediments which were eroded during these Pleistocene glaciations were deposited as large trough mouth fans and wedges off the western shelf margin. The Bjørnøya and Storfjorden trough mouth fans are some of these wedges, containing up to 4 km thick glacial accumulations (Smelror et al., 2009; Doré, 1995).

Cenozoic stratigraphic and depositional development

Due to later Neogene uplift and erosion of most of the Barents Shelf, Paleogene sediments are mostly preserved on Spitsbergen and in some western basins, whereas they have largely been removed on the central part of the Barents Shelf (Smelror et al., 2009). The eastern parts of the Barents Shelf are thought to have been uplifted continental highlands, or shallow marine during the Paleogene (Smelror et al., 2009).

A consequence of the opening of the Norwegian-Greenland Sea, during Eocene/Oligocene, was a rotational uplift of the eastern and northern Barents Shelf, and subsidence of the westernmost shelf (Worsley, 2008). Basins in the west, including the Harstad, Tromsø and Sørvestnaget basins, and the Vestbakken Volcanic Province, were all major sites of deposition during Eocene times, as eroded material from newly uplifted areas was transported towards the shelf edge to the west (Smelror et al., 2009).

Inner to outer shelf deposits seem to dominate the basins on the western Barents Shelf from Paleogene times (Sotbakken Group - Figure 2.3). The Paleocene strata is mostly claystone, whereas the overlying Eocene includes gravity flow deposited blocky sandstones, specifically in the Sørvestnaget Basin. In the Nordkapp and Hammerfest basins, Paleocene and Lower Eocene mudstones are found, unconformably overlying Lower Cretaceous units (Worsley, 2008). The claystone unit found in these basins is relatively thin in the Nordkapp Basin, and thickens westward throughout the Hammerfest Basin (180–770 m), Tromsø Basin (900 m), Bjørnøya Basin (1000 m) and Sørvestnaget Basin, where it reaches a thickness of over 2800 m (Ryseth et al., 2003; Worsley, 2008). The Finnmark and Bjarmeland platforms and the Loppa High, have had their Paleogene units removed by uplift and erosion, as represented by a base Quaternary unconformity (Smelror et al., 2009).

Between Miocene and Pleistocene the western Barents Shelf was repeatedly scoured by glaciers, removing large amounts of sediments from the shelf, and depositing them as clastic

Study area and geological background

wedges off the western margin (Worsley, 2008; Smelror et al., 2009). The repeated glacial erosion and isostatic uplift removed the largest amount of sediments in the northern parts of the shelf and around Svalbard (2–3 km), and less in the Hammerfest and southwestern sub-basin of the Nordkapp Basin, where around 2 km sediments were removed (Worsley, 2008; Smelror et al., 2009).

2.2 The Nordkapp Basin

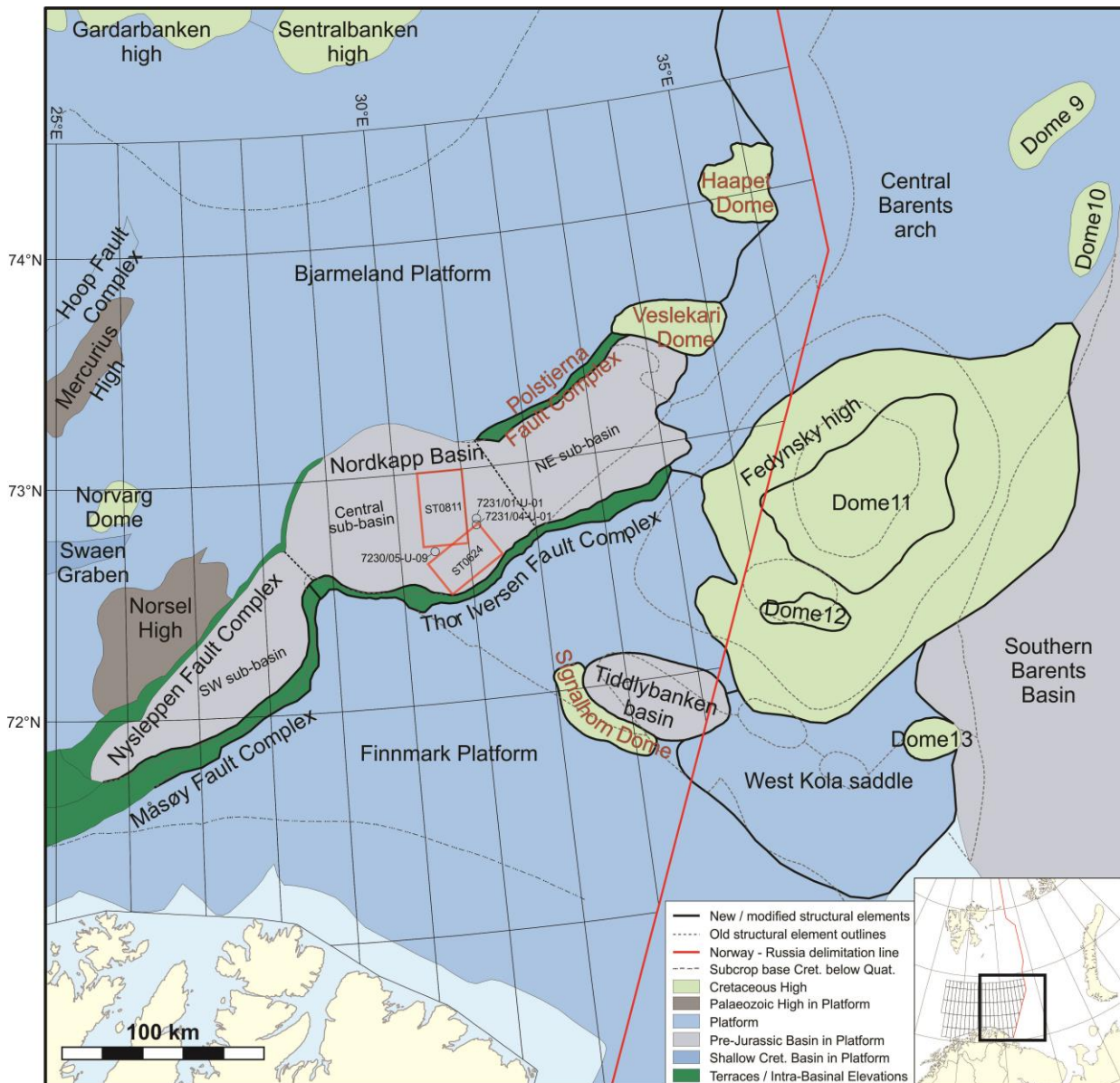


Figure 2.4. Structural map of the southern Barents Sea, after the disputed Norwegian-Russian naval border was established in 2010. The two 3D seismic surveys used in this study (ST0624 and ST0811) are marked with red rectangles. Modified after Mattingsdal et al. (2015).

The Nordkapp Basin is a deep, fault-bounded rift basin located in the eastern part of the Norwegian Barents Shelf (Figure 2.4). The basin is thought to have been initialized during post-Caledonian orogeny rifting events, during late Paleozoic time (Doré, 1995; Worsley, 2008). Like many of the other structural features in the western Barents Shelf related to the Caledonian orogeny (e.g. Ottar, Maud, Hammerfest basins), a similar NE/SW trend is also evident in fault trends along the margins of the Nordkapp Basin (Gabrielsen et al., 1990; Gernigon et al., 2014). The Nordkapp Basin contains some of the thickest accumulations of sedimentary sequences on the Barents Shelf, totaling 8 km above the basement (Smelror et al., 2009).

2.2.1 Basin fill development and stratigraphy

During Late Carboniferous and Early Permian time, the Barents Shelf was situated at around 20°N latitude, in an increasingly arid, tropical or subtropical climatic environment (Ahlborn and Stemmerik, 2015; Smelror et al., 2009). Although some carbonate shelves were found throughout the Barents Shelf in earlier ages, not until the Muscovian age did carbonate and evaporate deposition dominate the whole Barents Shelf. Carbonates and evaporites dominated the shelf until the middle Permian (Smelror et al., 2009). In the Nordkapp Basin, large salinas, or playas, which were formed during sea level lowstands, depositing large amounts of evaporates. Correlatively, a similar situation is thought to have occurred in the Sverdrup Basin in Arctic Canada, of approximately same age as the Nordkapp Basin (Worsley, 2008).

The basin was a major site for deposition during Triassic times, with deltaic sediments being sourced from the Uralian Mountains to the east, prograding northwestward across the Barents Shelf (Glørstad-Clark et al., 2010; Halland et al., 2011). Movement in the halite deposited during Late Paleozoic times started during Early Triassic (Halland et al., 2011; Koyi et al., 1993; Gabrielsen et al., 1990).

During the Late Triassic and until Middle Jurassic, the Nordkapp Basin, like large parts of the western Barents Shelf, saw a shift from the Triassic deltaic successions, to a shallow marine setting (Worsley, 2008). Relative sea levels rose during early Norian, opening up a proto-Atlantic seaway. Sandstones were still deposited in these shallow marine settings, although at a lower rate than in earlier Triassic (Worsley, 2008). Another regional transgression during Bathonian saw the shift from coarse to fine grained sediment deposition. The organic rich claystones of the Hekkingen Formation were deposited over large parts of the Barents Shelf, particularly thick in the Paleozoic basins, including the Nordkapp and Hammerfest Basins, indicating that these were sites of increased accommodation during the Jurassic (Worsley, 2008).

2.2.2 Basin segments and tectonic sub-elements in the Nordkapp Basin

The Nordkapp Basin is divided into two main segments: a southwestern and a northeastern basin, whereof the latter can further be divided into a central and a northeastern sub-basin (Figure 2.4). The general axis orientation of the whole basin is NE-SW trending, though the central part has a more E-W basin axis orientation (Gabrielsen et al., 1990). The basin is located in a basemental low between the Bjarmeland Platform to the northwest and the Finnmark Platform to the southeast. The southwestern sub-basin is bounded by the Måsøy

Study area and geological background

Fault Complex to the east and the Nysteppen Fault Complex to the south and west, and is described as an asymmetric half-graben structure (Figure 2.4) (Gudlaugsson et al., 1998). The central and northeastern sub-basins are bounded by the Nysteppen Fault Complex to the west, the Polstjerna Fault Complex to the north, and the Thor Iversen Fault Complex to the south and southeast (Figure 2.4). The central and northeastern basins have symmetrical graben structures, at least when defined at pre-Permian levels (Gabrielsen et al., 1990). An intrabasinal ridge separates the southwestern basin segment, from the northeast lying ones (Gudlaugsson et al., 1998).

As seen in Figure 2.4, the Nordkapp Basin is bounded on most sides by fault complexes. The Nysleppen Fault Complex bounds the southwestern sub-basin of the Nordkapp Basin to the west, to the Norsel High and Bjarmeland Platform. The fault complex has a NE-SW structural direction, and is composed of several fault sets of normal faults, throwing down the southeastern block (Gabrielsen et al., 1990; Gudlaugsson et al., 1998).

The Finnmark Platform bounds to the Nordkapp Basins southwestern sub-basin by the Måsøy Fault Complex, and to the central and northeastern sub-basins by the Thor Iversen Fault Complex (Figure 2.4). The fault complexes consist of normal faults, with the northern lying Nordkapp Basin being the downthrown block (Gudlaugsson et al., 1998). The Polstjerna Fault Complex bounds the northern margin of the northeastern sub-basin of the Nordkapp Basin, towards the northwest, to the Bjarmeland Platform (Figure 2.4).

2.2.3 Surrounding structural areas

As stated previously, the Nordkapp Basin is located in a basemental low between the stable Finnmark Platform to the southeast and the Bjarmeland Platform to the northwest (Figure 2.4).

The Finnmark Platform is bounded by the Caledonides exposed onshore Norway to the south. To the north, the Måsøy and Thor Iversen fault complexes separate the platform from the Nordkapp Basin. The western boundary of the Finnmark Platform is defined by the Troms-Finnmark Fault Complex, and the subcrop of Jurassic strata, terminating in the base Quaternary. Northeast, the platform is bounded by the Fedynsky high (Gabrielsen et al., 1990; Mattingsdal et al., 2015). Mesozoic strata on the platform dips towards the north, and subcrop to the south when it reaches the Upper Regional Unconformity (URU), left by Quaternary glaciation. Carbonate platforms of Permian age have been identified to the south and east of the Finnmark Platform, indicating a paleo shelf edge being positioned on the platform

Study area and geological background

(Gabrielsen et al., 1990). The platform is presumed to be underlain by a Precambrian and Paleozoic rock basement. Rifts and faults on the platform follow the Caledonian NE–SW orientation (Gabrielsen et al., 1990).

The Bjarmeland Platform is bounded by the Nordkapp and Hammerfest basins to the south, and by the Sentralbanken and Gardarbanken highs to the north. The Fingerdjupet Subbasin and Loppa High bound the platform to the west, and were parts of the platform before tectonism during the late Mesozoic (Gabrielsen et al., 1990). Other structural elements are part of the Bjarmeland Platform, including the Norsel and Mercurius highs, Svalis, Samson and Norvarg domes, Swaen Graben and Maud Basin. Sedimentary successions on the platform dip towards the south, and subcrop north into the URU.

2.2.4 Salt in the Nordkapp Basin

The Nordkapp Basin is characterised by the many salt domes and diapirs, penetrating and deforming large parts of the post-Paleozoic strata (Figure 1.1) (Gabrielsen et al., 1990). The original evaporites were deposited in the basin during the arid Moscovian, and mainly moved throughout Triassic (Smelror et al., 2009; Grimstad, 2016; Faleide et al., 1984; Nilsen et al., 1995). The original thickness of the salt deposits averaged between 1.0 and 1.8 km in the southwestern sub-basin, and between 2.3 and 3.1 km in the central sub basin. The maximum thickness of the salt layer are thought to have been 2.0–3.2 km in the southwestern sub-basin, and 4–5 km in the central basin (Gudlaugsson et al., 1998). Halokinetic sequences proximal to salt diapirs are potential stratigraphic hydrocarbon traps, making the mapping of salt and near salt structures of interest for the petroleum industry (Giles and Rowan, 2012). However, salt structures are known to cause some problems in seismic imaging, related to the very low density and high velocity of the salt minerals, and subsequently a large amount of energy lost at the sediment-salt interface (Chapter 1.3.4) (Rojo et al., 2016; Jackson and Hudec, 2017).

2.2.5 Previous studies of the Lower Cretaceous succession in the Nordkapp Basin

Nilsen *et al.* (1995) pointed out that between 1000 and 1500 m of Cretaceous sediment wedges were deposited and prograded without interruption over the salt diapir crests in the Nordkapp Basin. According to the authors, this indicated that there was little to no movement in the salt during the Early Cretaceous.

Dimitriou (2014) identified four distinct prograding units in the Lower Cretaceous strata, with internal clinoform reflections, spanning the eastern part of the western Barents Shelf. The

Study area and geological background

units were found to be separated by maximum flooding surfaces at their bottoms, and erosional surfaces at their tops. The source area for these prograding units was suggested to be uplifted terrain related to the High Arctic Large Igneous Province (HALIP) north of the Barents Shelf.

In a combined study of seismic, well and biostratigraphic data, Marin *et al.* (2017) subdivided the Lower Cretaceous succession of the Barents Shelf into seven genetic sequences (S0–S6), *sensu* Galloway (1989). The succession lies between the Base Cretaceous Unconformity (BCU) below, and Upper Regional Unconformity (URU) above. The sequences are bounded and defined by regional flooding surfaces (K0–K5). The sequences each span 5–10 Ma, which correspond to third-order sequences. For this study, the sequences S1–S3 are relevant, as they span the central sub-basin of the Nordkapp Basin. A short description of Sequences 1 to 3 in the Nordkapp Basin area, as presented by Marin *et al.* (2017), follows, with age data and Svalbard correlation by Grundvåg *et al.* (2017).

Sequence 1 is described as having continuous parallel reflectors, of medium to high amplitude. The upper boundary of the sequence, Surface K1, has a high amplitude, and is interpreted as a regional flooding surface. Clinoform reflectors were identified in the north-eastern part of the central Nordkapp sub-basin. The clinoforms prograde towards the southwest, are high relief sigmoidal in geometry, and have an average foreset angle of 1°. The height of the clinoforms increases towards the southwest, from 130 to 400 m, and they have a slightly rising trajectory. The clinoforms downlap on the BCU. Grundvåg *et al.* (2017) suggest that the Rurikfjellet Formation (Valanginian–Hauterivian/lower Barremian) onshore Svalbard, correlate to Sequence 1 (uppermost Valanginian/Hauterivian–lower Barremian).

Sequence 2 includes parallel continuous reflectors with medium amplitude in the Hammerfest Basin and clinoform prograding towards the southeast in the Fingerdjupet Subbasin and on the western Bjarmeland platform. In the Nordkapp Basin, S2 includes clinoforms prograding towards the southwest. These clinoforms do transition from the high-relief, low gradient clinoforms found in S1, to oblique clinoforms of 40–60 m height, with high-gradient foresets of 1.5°–4°, in S2. The trajectory of the clinoforms varies between flat, slightly falling and slightly rising. Towards the top of the sequence, the clinoforms are higher, between 60 and 105 m, are sigmoidal, and have low-gradient forests (<1°). A slightly rising trajectory and low amplitude reflectors also distinguish the upper part of the sequence from the rest. The upper boundary of S2, surface K2, has a medium to high amplitude, and is

Study area and geological background

interpreted as a regional flooding surface. Grundvåg *et al.* (2017) suggest a correlation between S2 (uppermost Barremian–upper Aptian) and the Helvetiafjellet Formation (lower Barremian-lower Aptian), and the Dalkjegla and Innkjegla members of the Carolinefjellet Formation (lower Aptian–upper Aptian) onshore Svalbard.

Sequence 3 has reflectors ranging between parallel continuous with medium amplitude, and chaotic. Clinofolds are described in S3 in the Hammerfest Basin, and on the Bjarmeland Platform, downlapping on the boundary surface K2 or the BCU. The upper bounding flooding surface of S3 is Surface K3, where the sequence is not eroded by the URU. In Grundvåg *et al.* (2017) it is suggested that S3 (uppermost Aptian–lower/middle Albian) is correlated to the Langstakken, Zillerberget and Schönrockfjellet members (upper Aptian–middle Albian) of the Carolinefjellet Formation onshore Svalbard.

3 Data and methods

3.1 Seismic data

The 3D seismic surveys used in this study were ST0624 and ST0811 (Figure 2.4, Figure 3.2), and were provided by the NPD. Both surveys were acquired for Statoil ASA (StatoilHydro ASA at the time of survey ST0811), in 2006 and 2008 respectively. Both surveys are categorized as ordinary 3D seismic surveys. Survey ST0624 covers approximately 770 km², and ST0811 covers approximately 1065 km² (Figure 3.2). The Petrel E&P Software Platform (Version 2016) by Schlumberger was used for seismic interpretation and visualization. The inline direction of ST0624 is in a NE-SW direction, with 12.51 m distance between each trace, and ST0811 has an inline direction of N-S, with 18.78 m between each trace. Both seismic datasets have a zero phase signal with normal polarity (Figure 3.1), as per the polarity display convention of Sheriff (2002).

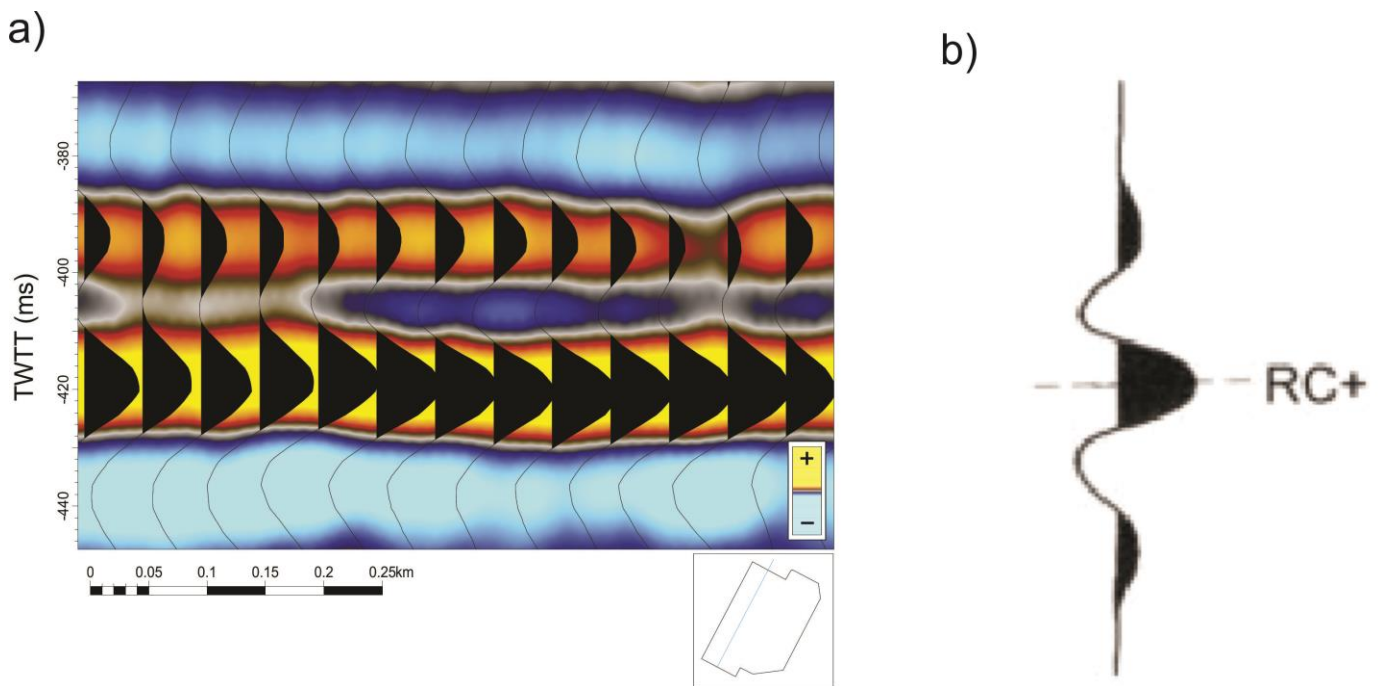


Figure 3.1. a) shows that the 3D seismic dataset ST0624 has a zero phase signal, with normal polarity. b) shows the exemplified zero phase signal with normal polarity, by Sheriff (2002).

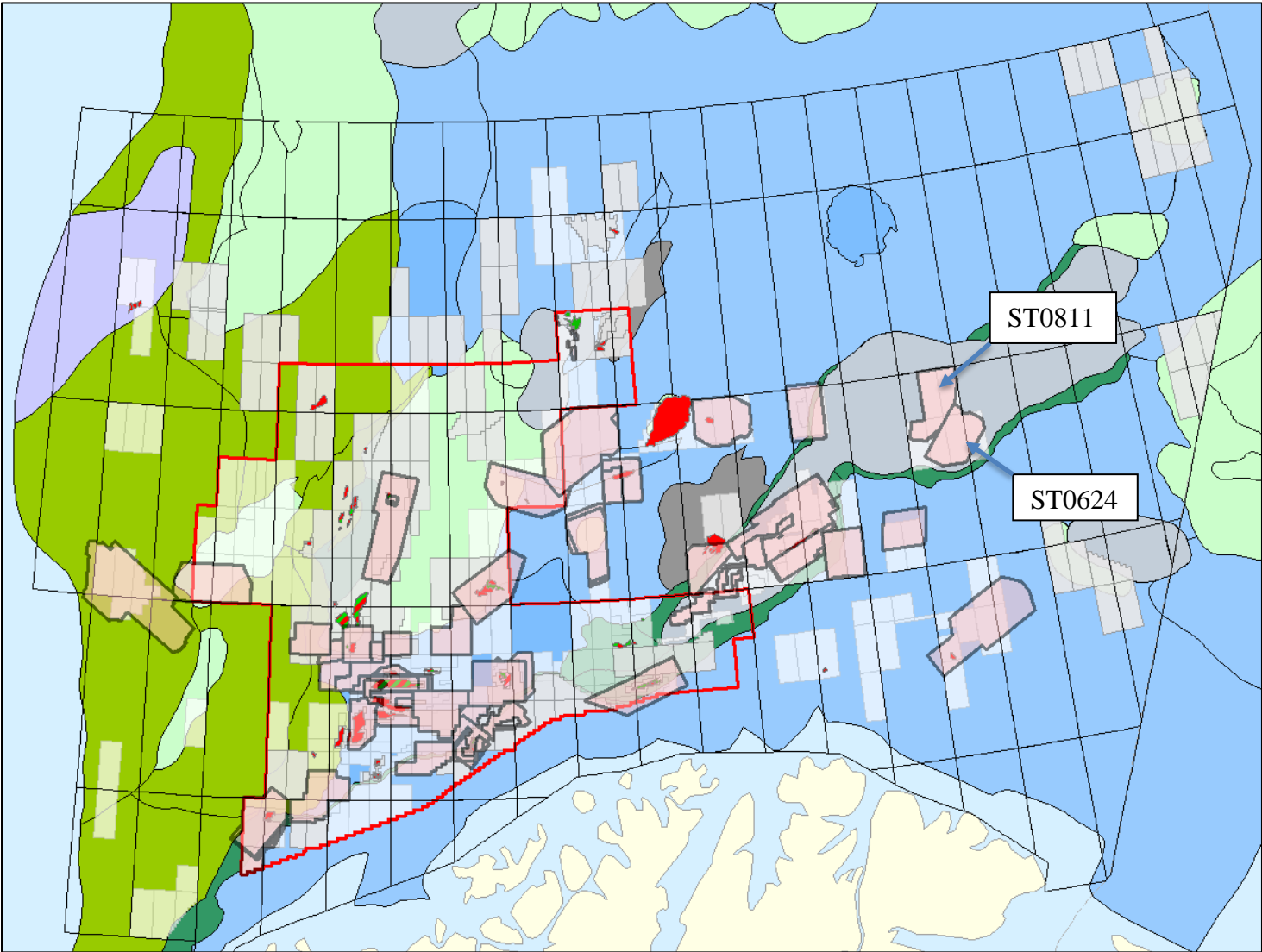


Figure 3.2. The location of the two 3D seismic surveys used during this thesis, ST0624 and ST0811, located in the central Nordkapp Basin, north off the Norwegian coast. Map provided by the NPD.

3.1.1 Seismic resolution

One difficulty in geological interpretation of reflective seismic data, is that objects of smaller sizes (e.g. thin rock layers) do not show up on seismic images. The required size of an object to be observable in seismic data is defined by the seismic resolution of the data. Seismic resolution is divided into a vertical resolution component (Equation 3.4, Equation 3.5) and a horizontal component (Equation 3.7). In 3D seismic data, an item can be recorded if it is larger than either the vertical or horizontal resolution.

$$Vr = \frac{1}{4} \lambda \tag{3.4}$$

Equation 3.4: The vertical resolution (Vr , m) is $\frac{1}{4}$ of the wavelength (λ).

$$\lambda = \frac{V}{F} \tag{3.5}$$

Equation 3.5: The wavelength (λ , m) can be calculated if the seismic velocity (V , m/s) and frequency (F , Hz) are known.

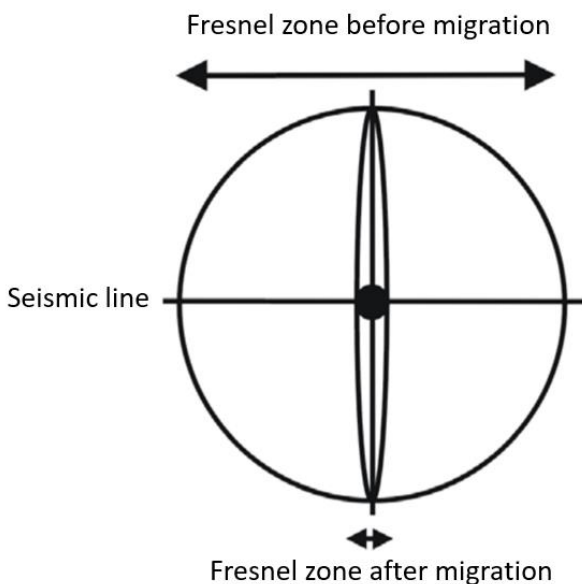


Figure 3.3. Illustration of how migration focuses the Fresnel zone. In 2D seismic data, the migrated Fresnel zone is an ellipsoid perpendicular to the seismic line. In 3D seismic data, the migrated Fresnel Zone is a small circle (centre of the illustration). From Brown (2011).

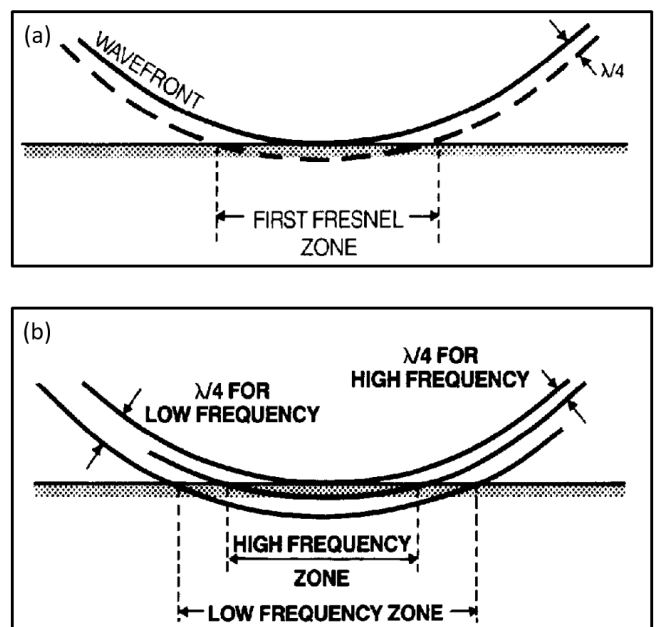


Figure 3.4. The Fresnel zone. (a) The Fresnel zone as defined as the area the wavefront of the seismic wave reaches within $\frac{1}{4}$ wavelength (λ). (b) The Fresnel zone becomes smaller with higher frequencies. Modified after Sheriff (1985).

Data and methods

The horizontal size of an item required to distinguish it from another item, is defined by the horizontal resolution of the seismic data. The horizontal resolution is described using the first Fresnel zone – i.e. the area on a horizon reached by the seismic wave front within half a cycle after the first wave reaches it (Figure 3.4) (Andreassen, 2009). The radius of the Fresnel zone is given by Equation 3.6.

$$rf = \frac{V}{2} \sqrt{\frac{TWTT}{F}} \quad (3.6)$$

Equation 3.6: The radius of the first Fresnel zone (rf, m) in unmigrated seismic data. V = velocity (m/s), TWTT = two-way travel time (s), F = dominant frequency (Hz).

When seismic data is migrated, the energy spread in the Fresnel zone is focused (Figure 3.3), reflections misplaced from dip are re-arranged, and the reflection patterns of points and edges are removed. The horizontal resolution of migrated seismic data is given by equation 3.7. The vertical and horizontal resolution of the two datasets used in this study are given in Table 2 and Table 3.

$$Hr = \frac{1}{4} \lambda \quad (3.7)$$

Equation 3.7: For migrated seismic data, the horizontal resolution (Hr, m) is 1/4 of the wavelength (λ).

Table 2. Approximate vertical (Vr) and horizontal (Hr) resolution of 3D seismic dataset ST0624. Velocities were calculated from the sonic transit time data of Well 7228/2-1S.

ST0624 TWTT (ms)	Dominant Frequency	Velocity (m/s)	Wavelength (m)	Hr (m)	Vr (m)
500	20	2500	125	31	31
1000	40	4400	110	28	28
1500	20	3800	190	48	48

Table 3. Approximate vertical (Vr) and horizontal (Hr) resolution of 3D seismic dataset ST0811. Velocities were calculated from the sonic transit time data of Well 7228/2-1S.

ST0811 TWTT (ms)	Dominant Frequency (Hz)	Velocity (m/s)	Wavelength (m)	Hr (m)	Vr (m)
500	28	2500	90	23	23
1000	20	4400	220	55	55
1500	25	3800	152	38	38

3.1.2 Artefacts and noise

Artefacts are objects found in the seismic dataset that do not represent any object in the real world, but are a result of the acquisition technique of the seismic data or the processing thereof. Artefacts in the form of acquisition footprints occur in both datasets, as lineations parallel to the inline direction (Figure 3.5). Acquisition footprint lineations are typical for 3D seismic data. Artefacts should be noted, as they may be interpreted as real features.

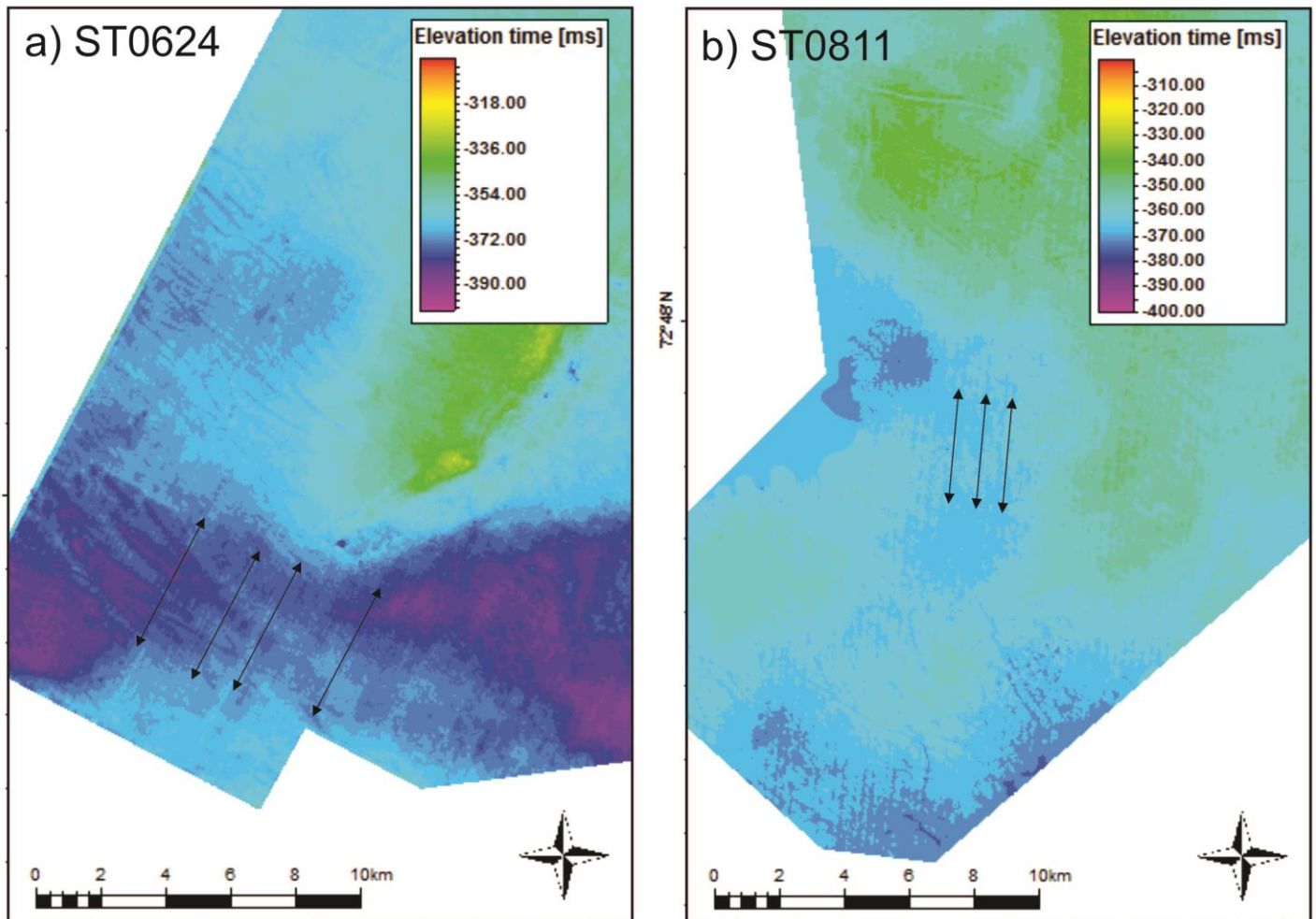


Figure 3.5. a) Acquisition footprint artefacts, marked with black arrows, in dataset ST0624. The lineations are in a N – S direction. B) Acquisition footprint artefacts in dataset ST0811. The lineations are in a NE – SW direction.

3.1.3 Fault interpretation

The integrated fault interpretation feature of Petrel 2016 was used in the identification and interpretation of faults in the seismic dataset. Radial expansion faults were extensively recognized and marked in the dataset around salt diapirs, in the Lower Cretaceous interval (Figure 3.6). Faults were interpreted where seismic reflectors were displaced upwards or downwards.

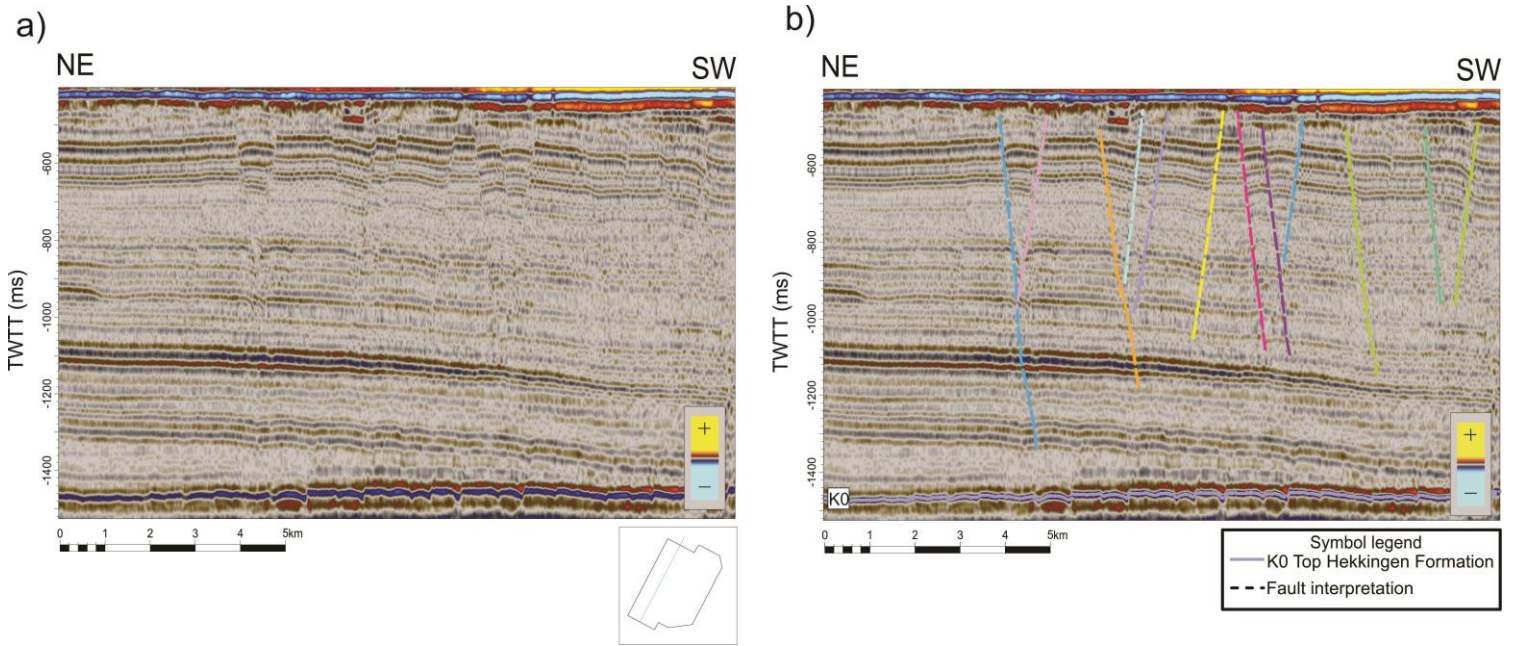


Figure 3.6. Examples of fault interpretation in Petrel 2016, in dataset ST0624. (a) shows the uninterpreted section, where displacement of reflectors can be observed. (b) shows the interpretations done using the integrated fault interpretation tool in the software.

3.2 Salt interpretation

A workflow described by Rojo *et al.* (2016) was used to identify and map salt diapirs in the study area. Following the salt interpretation workflow presented in the paper, three volume attributes were performed on the seismic data, consecutively: dip-guided structural smoothing, dip-illumination and variance. The attributes helped narrow down the location of the salt-sediment interface, on the boundaries of diapirs. As discussed in chapter 1.3.4, there are some challenges with interpreting salt in seismic data, and using tools (here attributes) to help interpret the salt bodies and surroundings with more confidence, are recommended.

3.3 Cores

3.3.1 Cores used in this study

Three shallow stratigraphic cores penetrating the Mesozoic stratigraphy in the Nordkapp Basin were used in this study: 7231/01-U-01, 7231/04-U-01 and 7230/05-U-09 (Table 4). Due to uplift and folding by salt diapirism, the Mesozoic strata is located at shallow levels beneath a Quaternary overburden, separated by the Upper Regional Unconformity (URU) (Bugge et al., 2002). Sedimentary successions down to Middle Triassic have been cored by shallow stratigraphic drilling on the Barents Shelf. The three cores investigated in this study were collected during a shallow stratigraphic drilling program by IKU Petroleum Research (now SINTEF Petroleum Research), in 1987 (SINTEF, 2009; NPD, 2017). Out of the twelve corehole sites in the survey, eleven were located on the periphery of salt diapirs. Corehole 7230/05-U-09 was drilled distant from salt, as this core targeted the youngest Mesozoic succession in the Nordkapp Basin (Bugge et al., 2002).

Figure 3.7 shows the coring location for the cores used in this study. Core 7231/01-U-01 and 7231/04-U-01 were taken east of the central Nordkapp sub-basin close to a salt diapir, whereas core 7230/05-U-09 was taken further west in the central sub-basin, away from any diapir.

Table 4. Overview of the cores used in the study. Metadata was gathered from Bugge et al. (2002) and the NPD FactPages for wellbore information (NPD, 2017).

Core number	Geographic co-ordinates	Water depth (m)	Quaternary overburden (m)	Core length (m)	Formations penetrated (Youngest to oldest)
7231/01-U-01	N 72°45'12.45" E 31°07'30.21"	278	36,3	55,7	Kolje, Klippfisk, Hekkingen
7231/04-U-01	N 72°44' 16.31" E 31°7'28.94"	280	37,7	58,0	Kolmule, Kolje
7230/05-U-09	N 72°37'22.44" E 30°22'31.41"	294	20,0	42,7	Kolmule

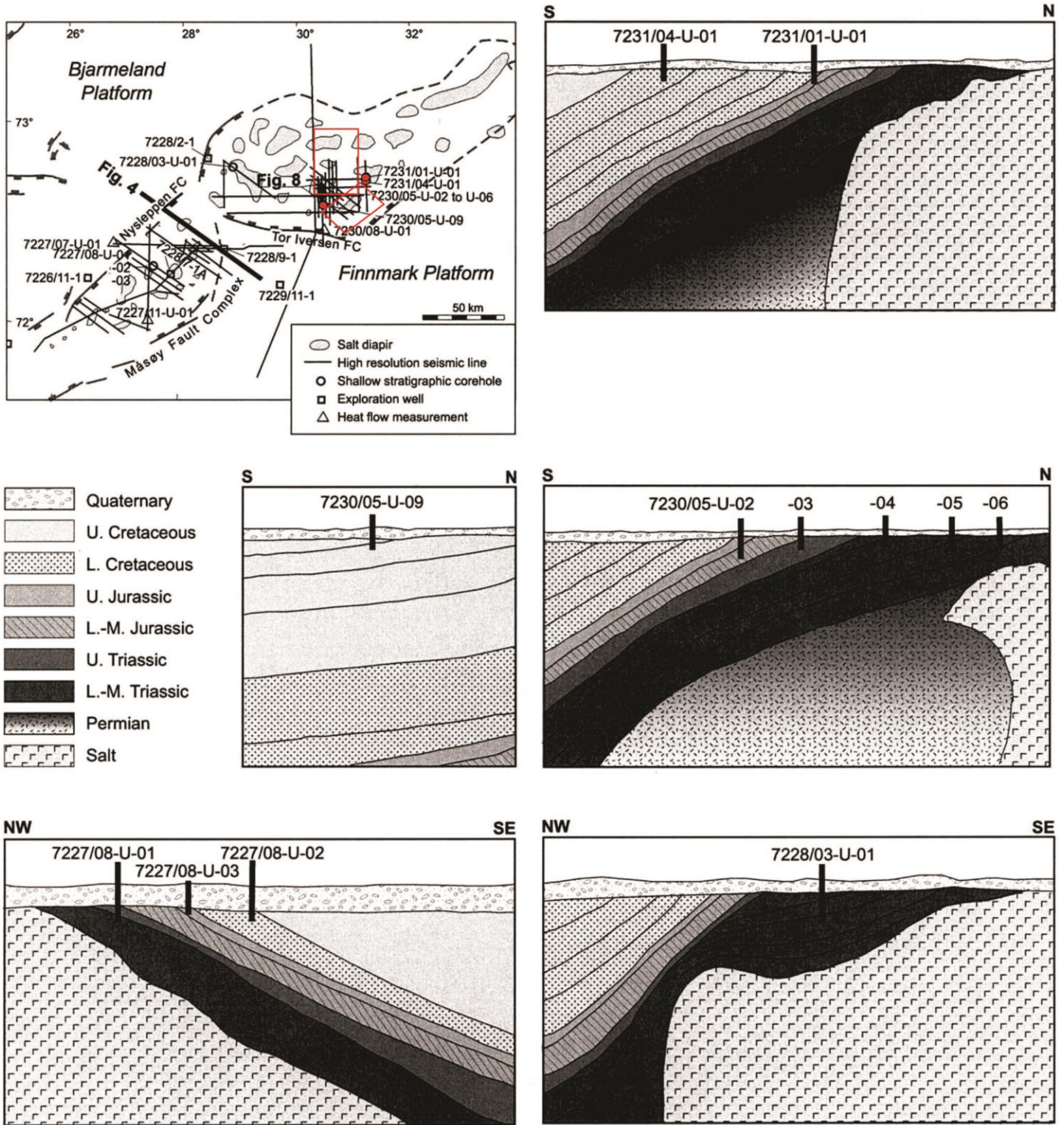


Figure 3.7. Location of the cores taken during the IKU Petroleum Research Shallow Stratigraphic Drilling projects between 1982 and 1993. The three cores used in this study are 7231/01-U-01, 7231/04-U-01 and 7230/05-U-09, marked with red dots. The approximate location of the seismic surveys used (ST0624 and ST0811) are highlighted with red rectangles. Modified from Bugge et al. (2002).

3.3.2 Shallow coring

The cores used in this study were retrieved as part of a shallow stratigraphic drilling program by IKU Petroleum Research between 1982 and 1993. The technique used during the program is described in detail in Rise and Sættem (1994). A roller cone drill bit was used to penetrate the Quaternary overburden. Subsequently, a diamond coring bit was used to continuously retrieve cores from the underlying strata, in 3 m segments, with a core diameter of 54.4 mm (Figure 3.8). The geophysical properties spectral gamma-ray intensity and horizontal sound velocity were measured in the cores after retrieval (Bugge et al., 2002). In the IKU shallow stratigraphic drilling program, it became standard to measure core hole geometry (caliper), gamma-ray, multichannel sonic, density, neutron porosity and dip/micro-resistivity with downhole logging tools in all holes after 1988 (Rise and Sættem, 1994).

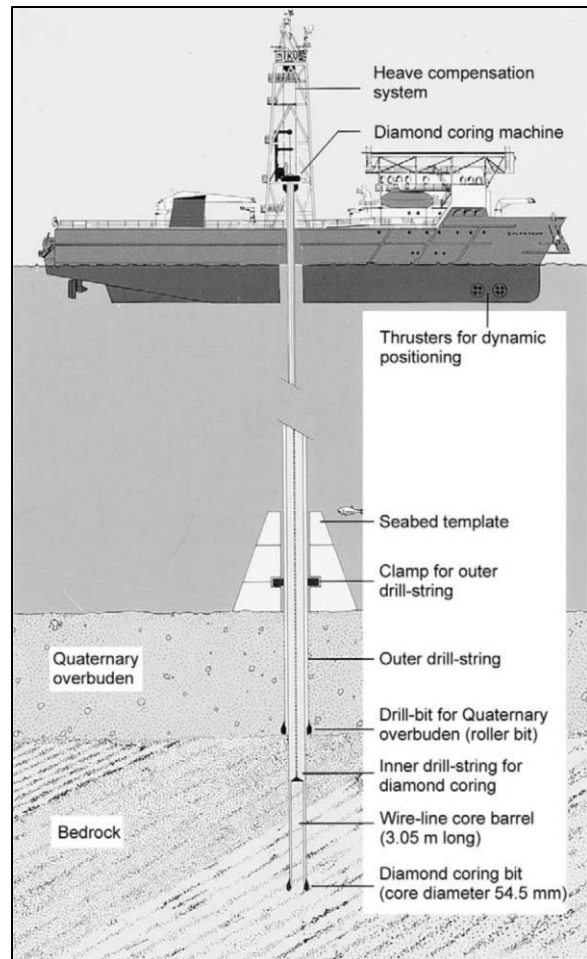


Figure 3.8 A sketch depicting the principle used during the shallow stratigraphic coring by IKU Petroleum Research (Rise and Sættem, 1994). Figure from Bugge et al. (2002)

3.3.3 Sedimentary logging parameters

As the main goal of use for the cores is to correlate them to the seismic data set, general sedimentological parameters were used during the descriptions of the cores. The focus while logging was on variations in lithology, grain size, color and, degree of bioturbation, sedimentary structures, type of trace fossils and macro fossils. Together these parameters were used to define facies associations, and subsequently correlated to the seismic dataset.

4 Results and findings

4.1 Salt

4.1.1 Salt diapirs in the study area

Seven salt structures are identified in the study area, affecting the Lower Cretaceous succession by pulling it up towards the diapir sides (Figure 4.1). Names used for salt structures observed in the two seismic datasets *sensu* Grimstad (2016). Structure D1 lies to the west of the study area and is not considered here (Grimstad, 2016). Structures D2, D4 and DS8 are only partially encompassed in the seismic data available, and therefore no full structure morphology is observed. A short description of each structure and their surroundings follows, summarized in Table 5.

Table 5. List of salt structures with influence on the Cretaceous stratigraphy in the seismic datasets ST0624 and ST0811, and properties of these.

Name	Locality in seismic data	Structure type	Morphology	Stratigraphic top reached / ms	Orientation
D2	ST0624: Southwest	Diapir	Undefined	Jurassic, -1500 ms	Undefined
D3	ST0624: Central	Diapir	Elongated	Sea bottom / Quaternary, -400 ms	NE–SW
D4	ST0624: North, ST0811: Southeast	Diapir	Undefined	Sea bottom / Quaternary, -400 ms	Undefined
DS4a	ST0811: South	Diapir system	Elongated	Jurassic, -600 ms	NE–SW
DS4b	ST0811: Central	Diapir system	Sub-circular	Sea bottom / Quaternary, -400 ms	N–S

Results and findings

DS7	ST0811: Central to north-west	Diapir system	Elongated	Sea bottom / Quaternary, -400 ms	E–W
DS8	ST0811: North	Diapir system	Elongated	Sea bottom / Quaternary, -400 ms	E–W

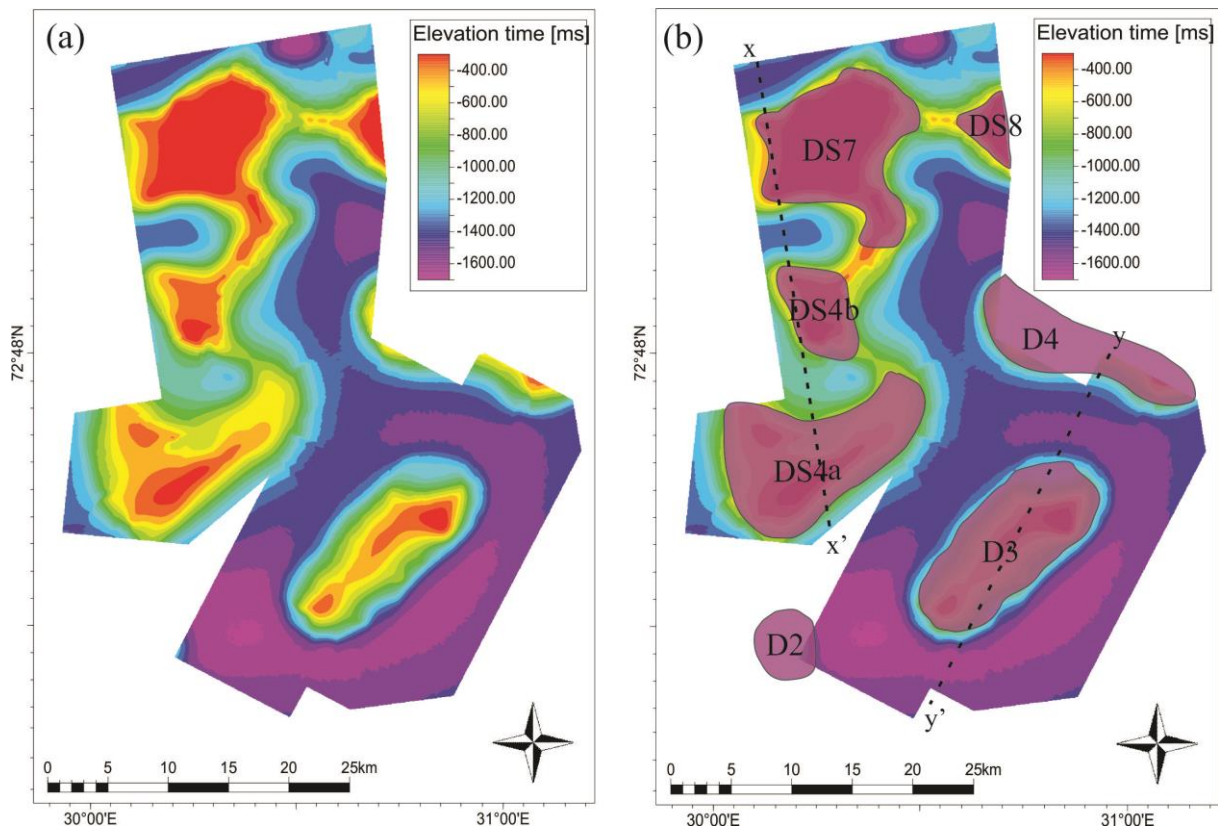


Figure 4.1. (a) Top Hekkingen Formation surface, cutting through the top of the diapirs, used to represent the salt structures in the seismic datasets. (b) Annotated Top Hekkingen Formation surface, with names of salt structures (Table 5), and location of seismic lines y – y' and x – x' (Figure 4.2)

D2

Salt diapir D2 is found partially in the southwestern corner of seismic dataset ST0624, where it reaches up to approximately -1500 ms (Figure 4.1). Overlying Upper Jurassic and Lower Cretaceous seismic sequences are steeply dipping near the underlying diapir, and drape it.

D3

Diapir D3 lies in the central part of dataset ST0624, and has an elliptical to elongated form, with the longest axis from northeast to southwest (Figure 4.1). The upper part of the diapir is about 15 km long, and 4 km across. Reflector J1 (Top Fuglen Formation equivalent) and

Results and findings

overlying Upper Jurassic and Lower Cretaceous sequences drape the sides of the diapir, until they terminate into the URU (Figure 4.2B).

D4

Salt diapir D4 is found partially in the northeastern part of seismic dataset ST0624, and on the southeast side of ST0811 (Figure 4.1). The diapir pierces the overburden all the way up to Quaternary units. The diapir flanks are draped by the Jurassic Hekkingen Formation as well as Lower Cretaceous seismic sequences, which are steeply dipping and terminate toplapping into the URU (Figure 4.2B).

DS4a and DS4b

Salt diapir DS4a lies in the southwest of dataset ST0811, and has an elongate to crescent shape (Figure 4.1). DS4b has a sub-circular form, and lies in the western part of ST0811 (Figure 4.1, Figure 4.2). Both diapirs are connected to a greater diapir system, together with DS7 and DS8, but divided by subbasins containing Jurassic and Lower Cretaceous units. DS4a is fully draped by Jurassic units, whereas DS4b pierces into the Quaternary, and surrounding Jurassic and Cretaceous sequences are pulled up and terminate into the URU.

DS7

Salt structure DS7 is an elongated diapir in the northwestern side of seismic dataset ST0811 (Figure 4.1, Figure 4.2). The diapir pierces the Lower Cretaceous sequences of focus in this study, and reaches the Quaternary overburden. Below surrounding subbasins, the diapir is connected to DS4a, DS4b, and DS8. The sides of the diapir are draped by seismic horizon J1 (Top Fuglen Formation equivalent), and overlying horizons and units (Figure 4.2D). The units flanking the diapir are pulled up, and terminate into the URU.

DS8

Salt structure DS8 is an elongated diapir in the northeastern side of seismic dataset ST0811, which reaches the Quaternary overburden (Figure 4.1). The sides of the diapir are draped by seismic horizon J1 (Top Fuglen Formation equivalent), and overlying surfaces and units (Figure 4.2D). The Upper Jurassic and Lower Cretaceous sequences flanking the diapir are pulled up, and terminate into the URU.

Results and findings

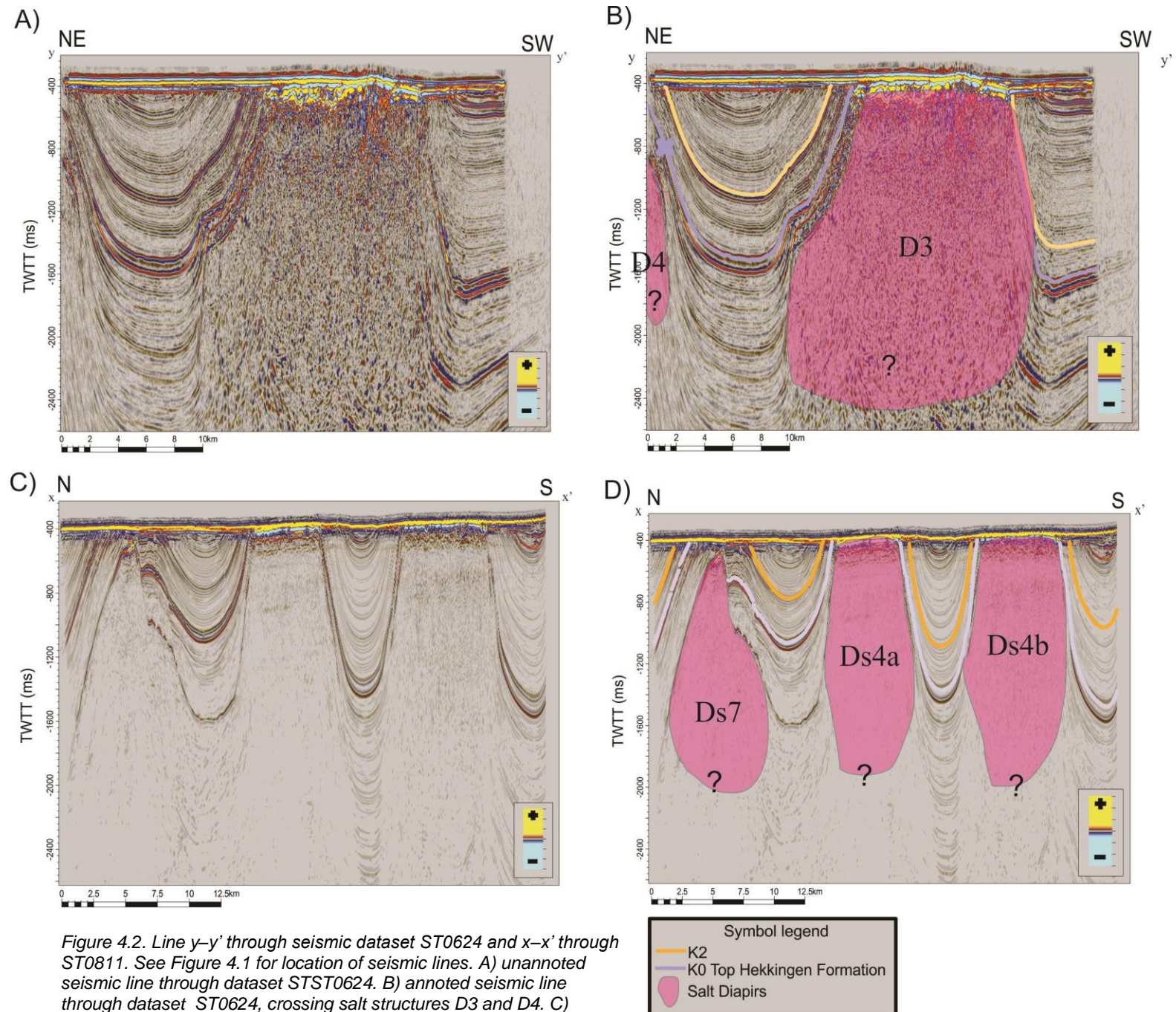
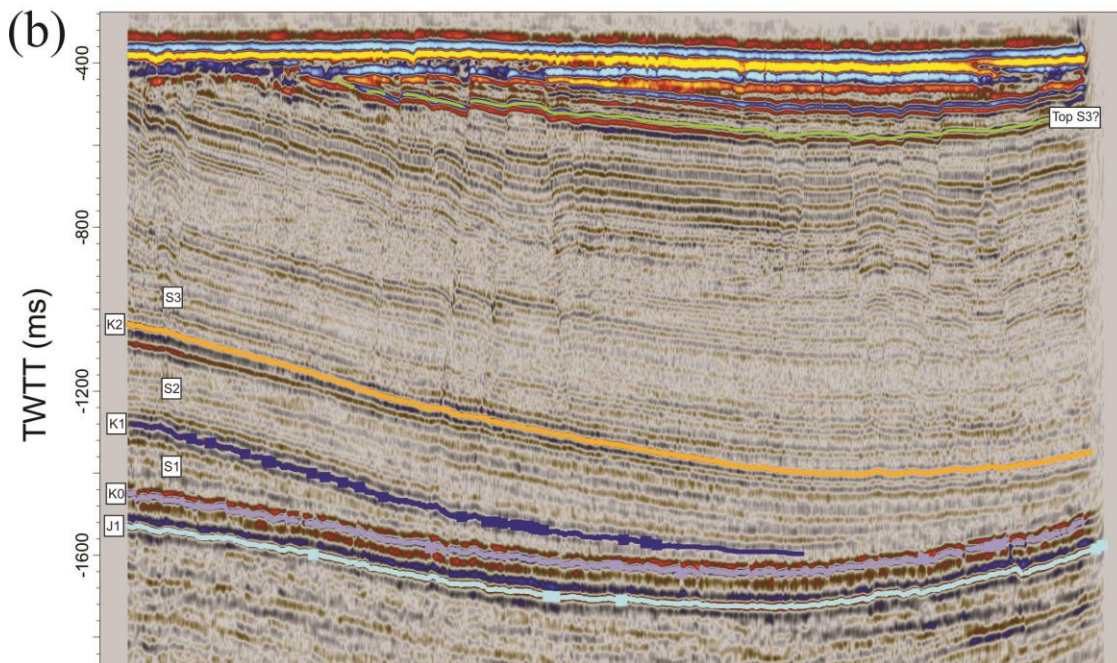
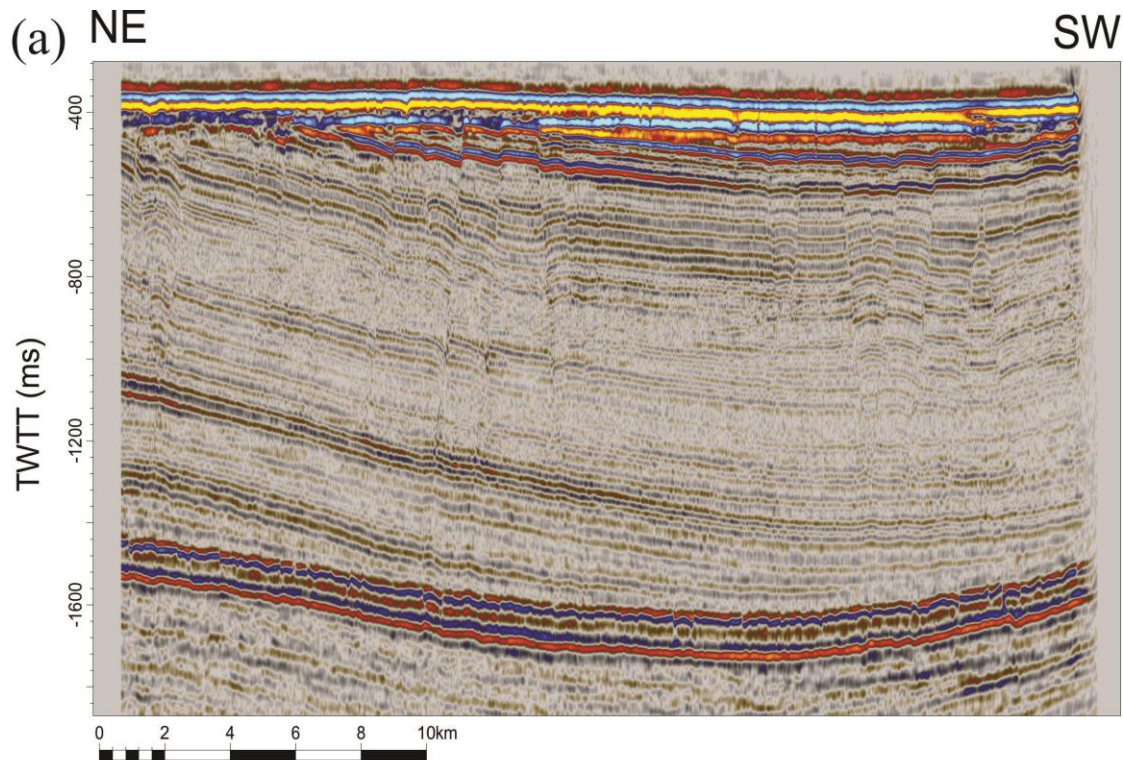


Figure 4.2. Line $y-y'$ through seismic dataset ST0624 and $x-x'$ through ST0811. See Figure 4.1 for location of seismic lines. A) unannotated seismic line through dataset ST0624. B) annotated seismic line through dataset ST0624, crossing salt structures D3 and D4. C) unannotated seismic line through dataset ST0811. D) annotated seismic line through dataset ST0811, crossing salt structures DS4a, DS4b and DS7.

4.2 Reflectors

The stratigraphy is based on corresponding flooding surfaces and sequences described by Marin *et al.* (2017).



Symbol legend	
	J1 Top Fuglen Formation
	K0 Top Hekkingen Formation
	K1
	K2
	S1
	S2
	S3
	Top S3?

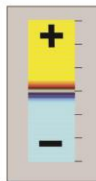
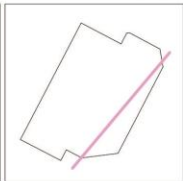


Figure 4.3. Key seismic horizons and sequences interpreted across the two 3D seismic datasets ST0624 and ST0811. (a) Uninterpreted random seismic line from ST0624. (b) Interpreted random seismic line from ST0624.

Results and findings

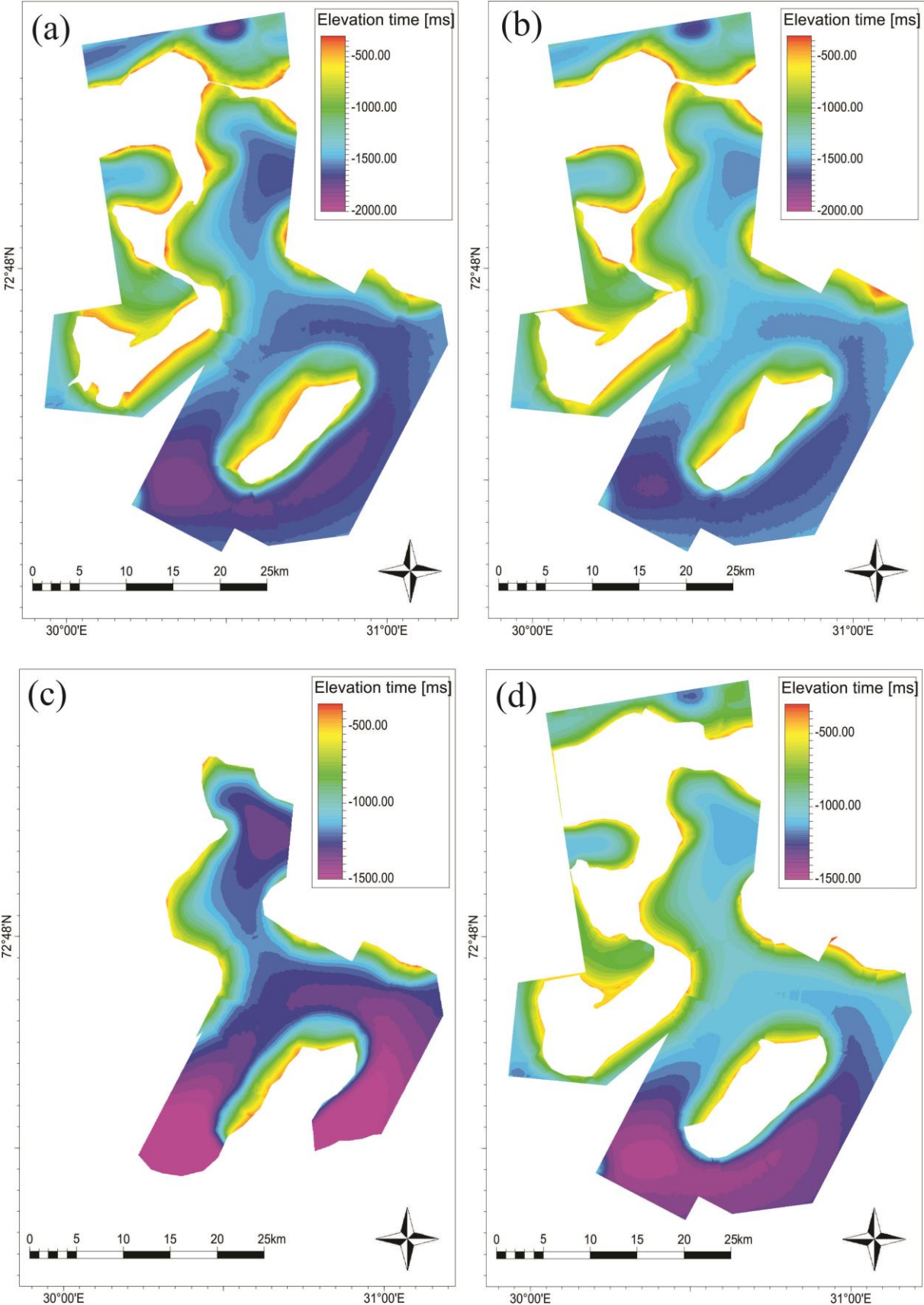


Figure 4.4. Time structure maps for key horizons interpreted in seismic datasets ST0624 and ST0811. (a) Time structure map J1. (b) Time structure map K0. (c) Time structure map K1. (d) Time structure map K2.

4.2.1 Upper Jurassic horizons

J1 – Top Fuglen Formation horizon

The Lower Cretaceous succession in the Nordkapp Basin is bounded below by the Upper Jurassic Fuglen and Hekkingen formations, of which Fuglen Formation is the oldest. The Top Fuglen Formation reflector (J1) is a high amplitude peak reflector in both datasets and is highly continuous (Figure 4.3). The reflector dips towards the south–southwest in the basins, and lies at approximately -1800 ms TWTT at its lowest in dataset ST0624. Around salt diapirs J1 is pulled up, at times eroded by the Upper Regional Unconformity (URU) between -300 and -400 ms TWTT.

K0 – Top Hekkingen Formation horizon and the Base Cretaceous Unconformity (BCU)

The Top Hekkingen Formation horizon (K0) is a high amplitude trough horizon, with moderately high continuity, in both datasets (Figure 4.3). The horizon dips towards the south–southwest, and is at its lowest at -1700 ms TWTT in dataset ST0624. In dataset ST0811, the K0 also reaches approximately -1700 ms TWTT in the northernmost rim synclinal basin. The continuity of the reflector is disrupted by small faults and fractures, attributed to the Base Cretaceous Unconformity (BCU). In proximity of salt diapirs the reflector is pulled up and eroded by the URU. Directly above surface K0 is a high amplitude peak horizon with high continuity, representing the Klippfisk Formation. This formation was also observed in shallow stratigraphic core 7231/01-U-01 (Figure 4.6), where a 4.5 m carbonate unit lies unconform above the black shales of the Hekkingen Formation.

4.2.2 Intra Lower Cretaceous horizons

K1

The K1 horizon is a low amplitude peak horizon, which spans both datasets (Figure 4.3). In both datasets the horizon has a moderate continuity, occasionally varying from high to low. K1 dips towards the south–southwest in dataset ST0624 where it laps down onto K0, and into the central rim synclinal in dataset ST0811. At its deepest area, the reflector almost reaches -1650 ms TWTT, in the south-western part of ST0624. Near salt diapirs the horizon is steeply dipping and eroded by the URU.

K2

K2 is a high amplitude peak reflector, found in both datasets (Figure 4.3). The reflector maintains a high continuity in shallow areas, but decreases to a moderate level in the deeper parts of dataset ST0624. It dips towards the south–southwest in ST0624 reaching nearly -

Results and findings

1500 ms TWTT, and into the central basin in ST0811. Close to salt diapirs the horizon is pulled up and eroded by the URU.

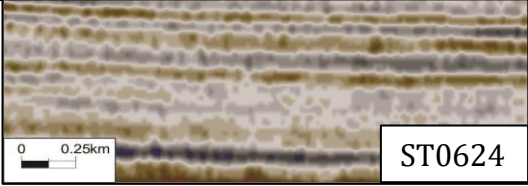
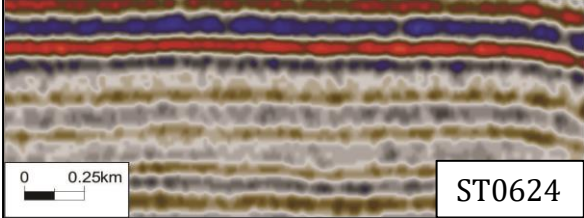
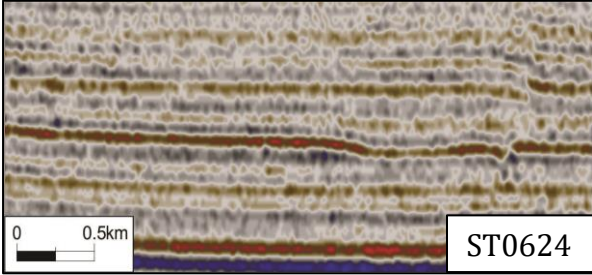
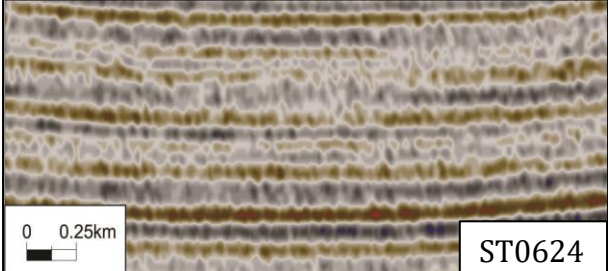
4.2.3 Upper Regional Unconformity (URU)

The Upper Regional Unconformity is represented by a high amplitude peak reflector in both datasets (Figure 4.3). The reflector dips slightly towards the south, lying between -375 ms TWTT in the very north of ST0824, and -450 ms TWTT in the south of ST0624. All the Lower Cretaceous horizons described above top lap into this plane towards basin edges.

4.3 Seismic Sequences

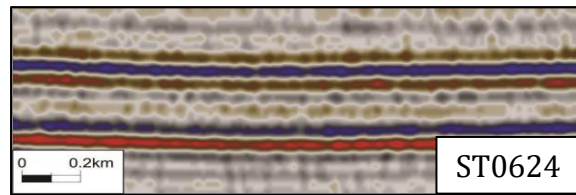
The Lower Cretaceous succession in the two seismic datasets can be divided into seismic units, or sequences, bounded by the key surfaces described in the previous chapter. The Lower Cretaceous sequences are defined by Marin *et al.* (2017), and dated by Grundvåg *et al.* (2017). Age data and formation equivalency for cores is gathered from Bugge *et al.* (2002). Typically observed facies patterns are summarized in Table 6.

Table 6. Overview of seismic facies observed in seismic data ST0624 and ST0811.

Seismic Facies	Description	Example from seismic data
SF1	Parallel simple stratified reflection configuration, moderate to low continuity, moderate to low amplitude strength	
SF2	Parallel simple stratified reflection configuration, moderate to high continuity, moderate to high amplitude strength	
SF3	Parallel simple stratified reflection configuration, moderate to high continuity, moderate amplitude strength	
SF4	Parallel simple stratified reflection configuration, continuity varies between reflectors from moderate to low, amplitude strength varies between high and low	

Results and findings

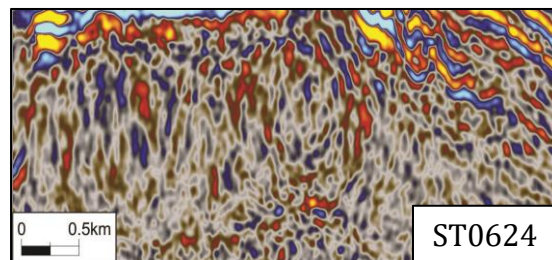
SF5 Parallel simple stratified reflection configuration, high continuity, moderate to high amplitude strength



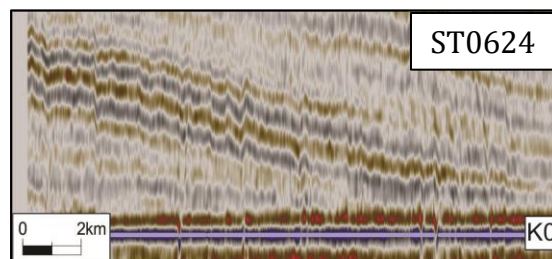
SF6 Varied reflection configuration between simple stratified parallel and reflection free, discontinuous, low amplitude strength



SF7 Chaotic reflection configuration, discontinuous, amplitude strength varies between low and high



SF8 Clinoform reflection configuration, continuity varies between reflectors from moderate to low, amplitude strength varies between moderate and low



4.3.1 Jurassic Sequence – JS1

Seismic description of JS1

The seismic unit Jurassic Sequence 1 (JS1) is bounded by surface J1 beneath, and K0 above. JS1 is dominated by seismic facies SF2 in dataset ST0624, and SF6 in ST0811 (Table 6). The sequence is distinctly even in time thickness in the basins, keeping at around 80 ms, but thins greatly towards salt diapirs, where the two bounding surfaces often run parallel adjacent to each other, until they top lap into the URU.

Sequence JS1 (Figure 4.5) keeps a near constant time thickness in the main basin, surrounding diapir D3, and between D4 and the DS4-DS7-DS8 diapir system. Towards diapir flanks however, the unit thins greatly, until the upper (K0) and lower (J1) boundary reflectors lie alongside each other.

Core description of JS1

JS1 occurs in shallow stratigraphic core 7231/01-U-01 (Figure 4.6), between 64.5 m and 92.8 m depth, as a finely laminated black shale (FA1 - Table 7). Some shell fragments occur in the unit.

Depositional environment of JS1

Seismic unit JS1, between the surfaces of K0 (Top Hekkingen Formation) above and J1 (Top Fuglen Formation) below, is interpreted to be the Hekkingen Formation all across the study area. The finely laminated black shale suggests that the unit was deposited in a marine basin with anoxic conditions.

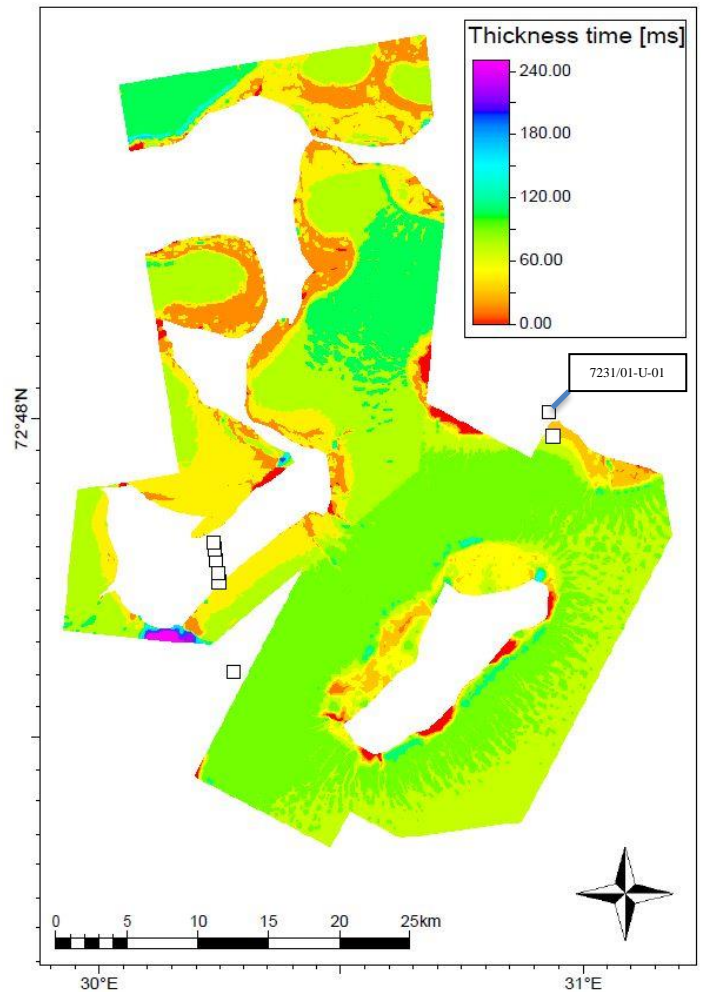


Figure 4.5 Time thickness map for Jurassic sequence 1 (JS1) in seismic dataset ST0624 and ST0811, in the central subbasin of the Nordkapp Basin.

7231/01-U-01 1:250

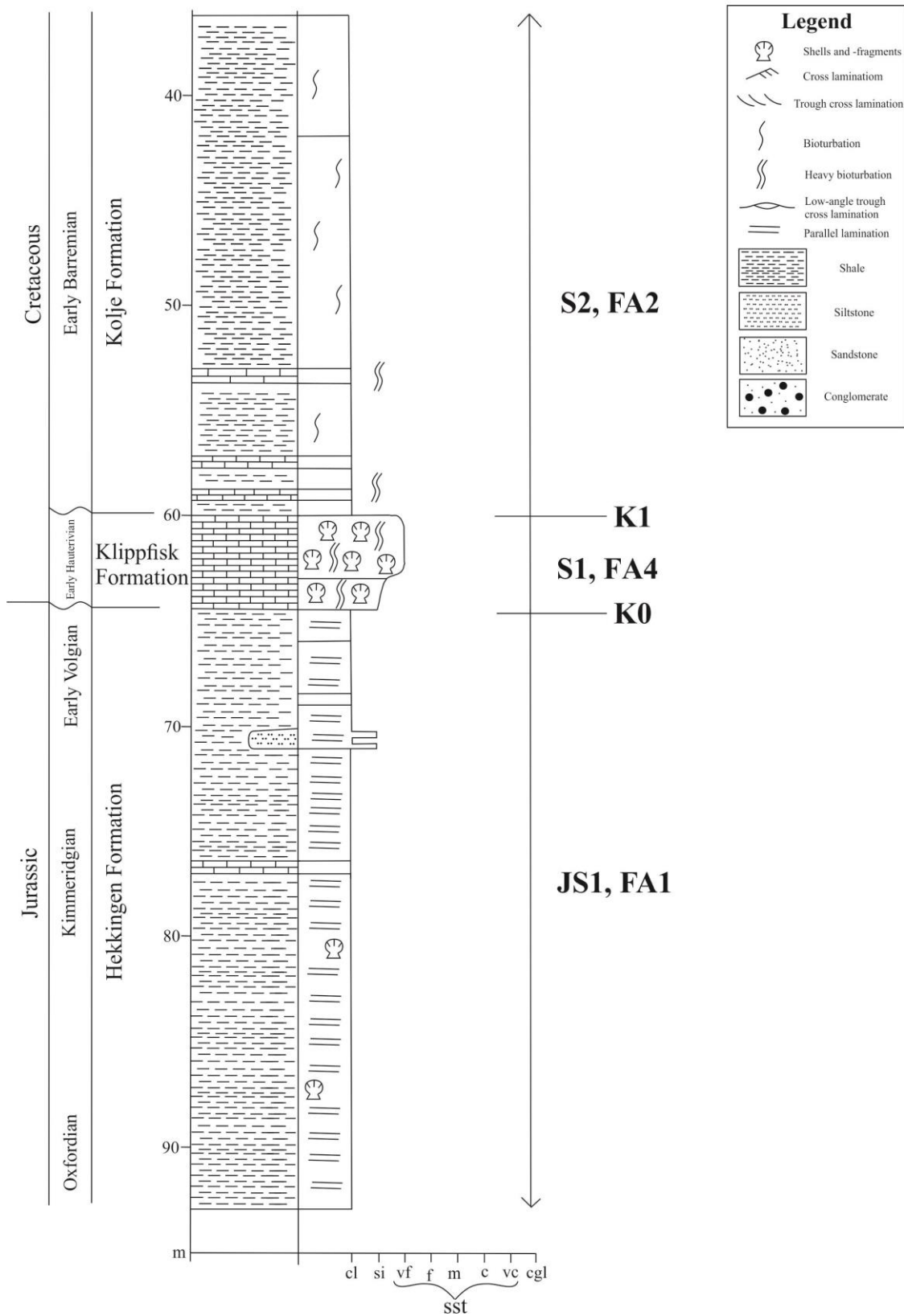


Figure 4.6. Log of shallow stratigraphic core 7231/01-U-01. The core penetrates the Hekkingen, Klippfisk and Kolje formations. The upper part of the core corresponds to clinoform toesets of S2 (Grundvåg et al., 2017; Marin et al., 2017). For facies associations (FA) see Table 7.

7231/04-U-01 1:250

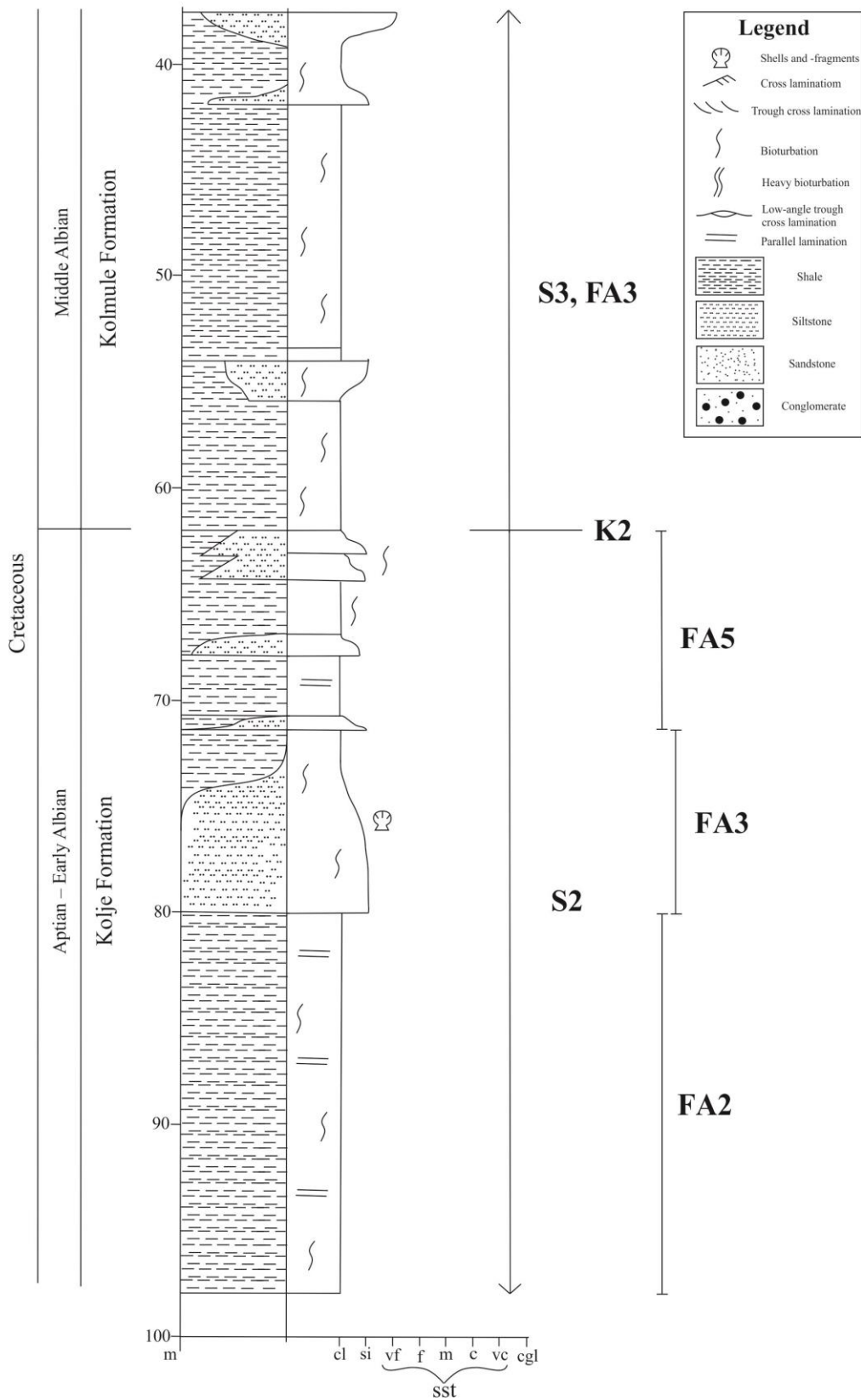








Figure 4.7. Log of shallow stratigraphic core 7231/04-U-01. The lower part of the core corresponds to S2. The upper part of the core corresponds to S3. The formation boundary between the Kolje and Kolmule formations corresponds to the sequence boundary and flooding surface K2 (Marin et al., 2017; Grundvåg et al., 2017). For facies associations (FA) see Table 7.

Results and findings


Table 7 Sedimentary facies observed in the shallow stratigraphic cores 7231/01-U-01, 7231/04-U-01 and 7230/05-U-09.

Name	Sedimentary Facies – Depositional Environment	Lithology	Description	Core occurrence	Example pictures from cores
FA1	Marine basin, possibly restricted	Black shale	Fine laminated black shale, fragments of shells, horizons of siderite cementation, lack of bioturbation	7231/01-U-01: 64.5–92.8 m	
FA2	Outer shelf	Grey claystone	Bioturbated grey to dark grey claystone, fragments of shells	7231/01-U-01: 36.2–59.9 m 7231/04-U-01: 79.6–97.3 m	
FA3	Middle shelf	Grey claystone and siltstone	Bioturbated dark grey to grey claystone and grey to light grey siltstone, parallel lamination, fragments of shells	7231/04-U-01: 37.2–62.5 m, 71.5–79.6 m	

Results and findings

<p>FA4</p>	<p>Starved carbonate shelf</p>	<p>Nodular carbonate wackestone and packstone</p>	<p>Nodular carbonate comprising green-grey wackestone and green-beige packstone</p>	<p>7231/01-U-01: 59.9–64.5 m</p>	
<p>FA5</p>	<p>Shallow marine to inner shelf</p>	<p>Light grey siltstone and grey very fine grained sandstone</p>	<p>Bioturbated light grey siltstone and grey very fine sandstone, fragments of shells</p>	<p>7231/04-U-01: 62.5–71.5 m 7230/05-U-09: 56.2–66 m</p>	
<p>FA6</p>	<p>Shoreface</p>	<p>Very fine to fine grained sandstone</p>	<p>Very fine to fine sandstone with low angle trough cross lamination, trough cross lamination, parallel lamination, bioturbation, fragments of shells</p>	<p>7230/05-U-09: 20–44 m, 46.3–56.2 m, 66–75.2 m</p>	

Results and findings

FA7	Lagoonal	Claystone, siltstone, very fine grained sandstone	Heterolithic unit comprising grey claystone, siltstone and very fine trough cross laminated sandstone, heavy bioturbation	7230/05-U-09: 44-46.3 m	
-----	----------	---	---	----------------------------	---

4.3.2 Sequence 1 – S1

Seismic description of S1

Sequence 1 (S1) is bounded by surface K0 beneath, and K1 above. S1 is dominated by seismic facies SF1 and SF8 in dataset ST0624, and SF6 in ST0811 (Figure 4.3) (Table 6). The unit thins significantly towards the southwest, where internal reflectors of the unit downlap onto surface K0, and the unit pinches out. Internal reflectors vary between discontinuous, and moderately continuous. The amplitude strength of internal reflectors vary between moderate and low. The lowermost internal reflector in S1 is a high amplitude, moderately continuous peak reflector, directly overlying K0. S1 is thickest in the northeast in the datasets, in the basins, where the unit reaches about 200 ms TWTT

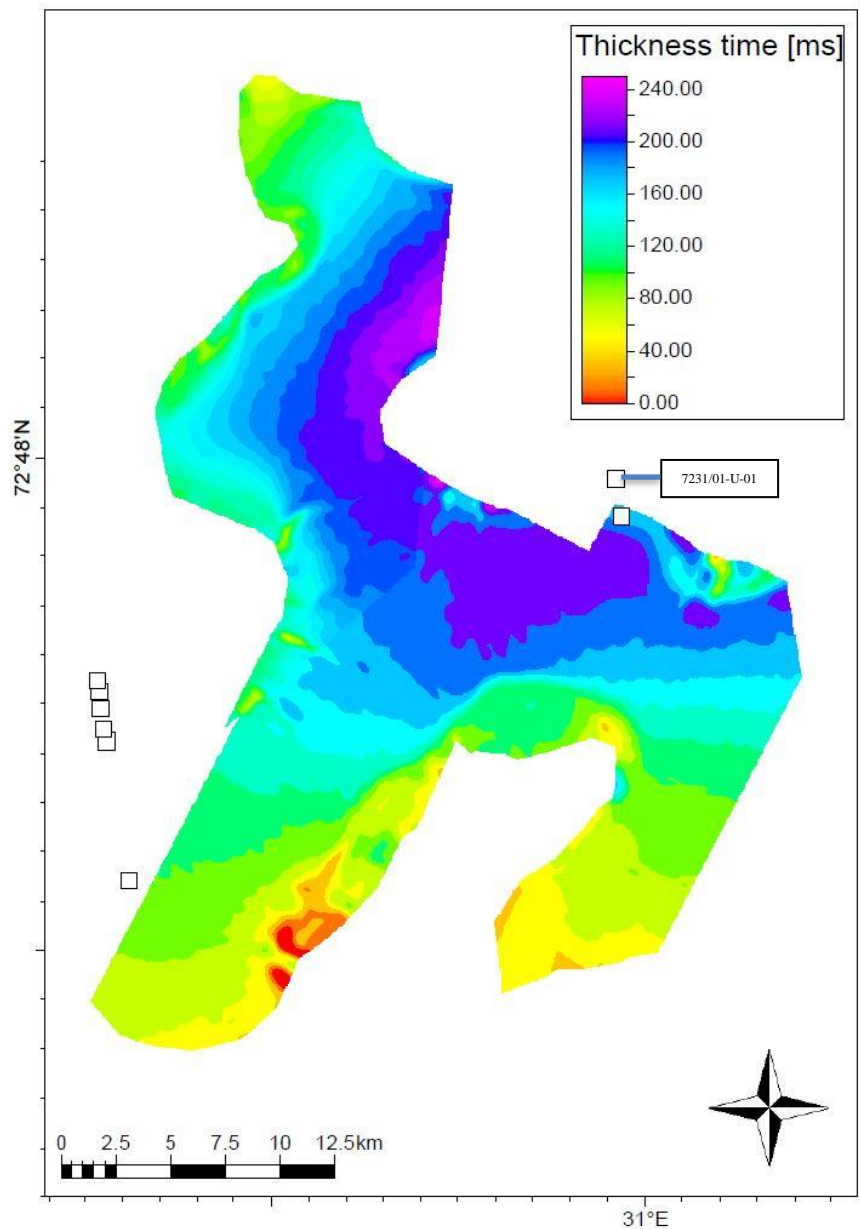


Figure 4.8 Time thickness map for Sequence 1 (S1) in seismic dataset ST0624 and ST0811, in the central subbasin of the Nordkapp Basin.

Results and findings

thickness. Towards salt diapirs internal reflectors in the unit onlap onto surface K0, and the unit thins in time thickness to 80–120 ms.

In the main basin, the time thickness of sequence S1 (Figure 4.8) diminishes greatly towards the southwest, as the unit downlaps onto the lower boundary K0. The depocenter of the unit in the study area is in the main basin, to the northeast. The unit thins towards salt diapir system DS4-DS7.

Depositional environment of S1

Dipping reflectors in S1 downlapping onto K0, are interpreted to be the distal parts of low angle clinoform units, as the unit wedges out in dataset ST0624. The high amplitude reflector at the bottom of S1, overlying K0, is thought to represent the carbonate Klippfisk Formation, observed in core 7231/01-U-01 (59.9–64.5 m, Figure 4.6). Thinning of the unit towards salt diapirs may be related to salt activity during deposition of the unit.

4.3.3 Sequence 2 – S2

Seismic description of S2

Sequence 2 (S2) is bounded by surface K1 and K0 beneath, and K2 above. The seismic facies dominating the unit are SF2 in dataset ST0624, and SF6 in ST0811. The internal reflectors in the sequence have a parallel simple stratified reflection configuration, moderate to high continuity and moderate to high amplitude strength. The unit runs parallel to S1 underneath, until S1 pinches out on surface K0. K0 defines the base limiting surface of S2. The unit generally has a TWTT thickness between 190 and 250 ms, thinning

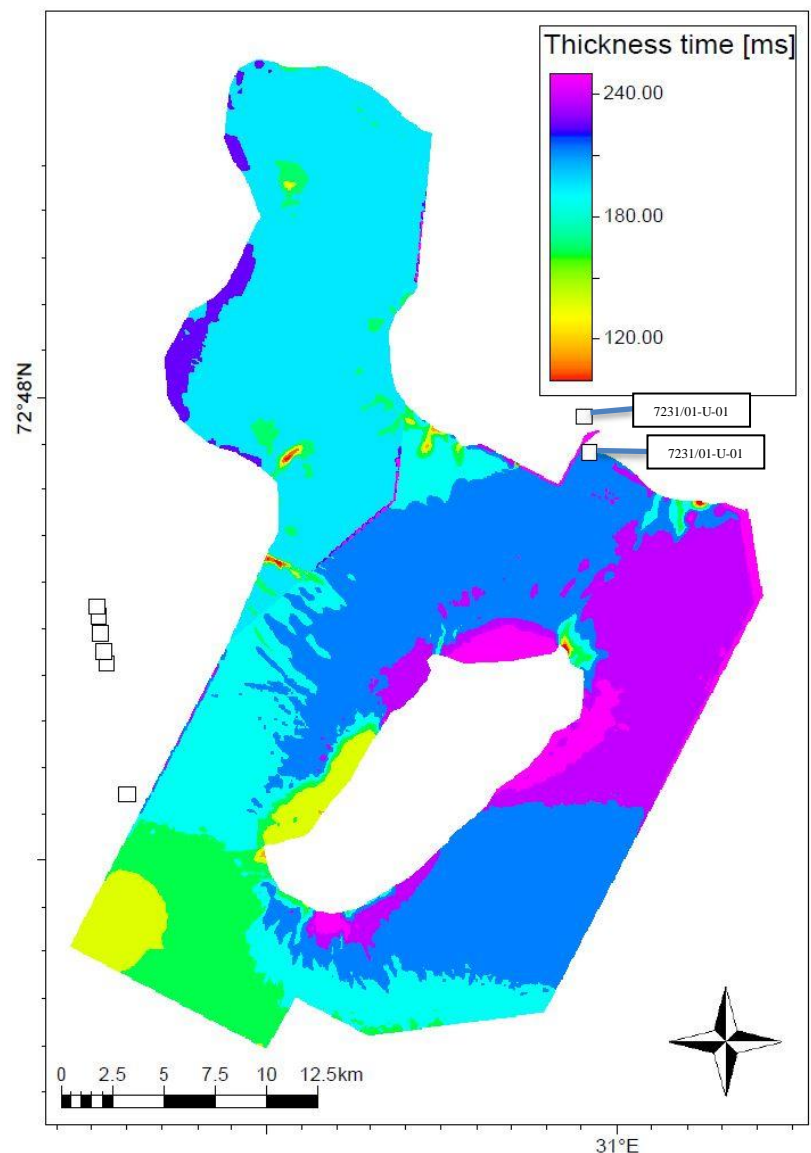


Figure 4.9 Time thickness map for Sequence 2 (S2) in seismic dataset ST0624 and ST0811, in the central subbasin of the Nordkapp Basin.

Results and findings

slightly towards the southwest in ST0624, and the main basin of ST0811.

The time thickness of unit S2 (Figure 4.9) is relatively constant in the main basin between salt diapir D4 and the DS4-DS7 system, and on the western flanks of diapir D3. The unit has a depocenter (maximum thickness) northeast of diapir D3, reaching approximately 250 ms TWTT. The unit thickness decreases towards the southwest in the study area, down to approximately 150 ms, southwest of D3.

Core description of S2

Sequence 2 (S2) occurs in shallow stratigraphic cores 7231/01-U-01 (Figure 4.6) and 7231/04-U-01 (Figure 4.7).

In core 7231/01-U-01 the sequence is seen as a bioturbated grey claystone between 36.2 m and 59.9 m depth (FA2 - Table 7). Within the grey shale, intervals of heavy bioturbated siderite cementation occur (Figure 4.6). The lower half of core 7231/04-U-01, between 62.5 m and 97.3 m depth, comprises of bioturbated and laminated dark grey claystone (FA2 - Table 7). Increasingly more intervals of lighter grey clayey siltstone occur (FA3 - Table 7), up to 62.5m. Single shell fragments occur (Figure 4.7).

Depositional environment of S2

In core 7231/01-U-01 the grey claystone corresponds to parts the Kolje Formation (Bugge et al., 2002), and toesets in the lower part of S2 (Grundvåg et al., 2017). The bioturbated grey claystone is interpreted to be deposited in an outer marine shelf environment. Intervals of siderite cementation are thought to represent times of extra slow sedimentation.

The lower part of core 7231/04-U-01, between 62.5 m and 97.3 m depth, corresponds to the upper part of the Kolje Formation, and to S2 (Bugge et al., 2002; Grundvåg et al., 2017). The upper part of the core corresponds to the lower part of the Kolmule Formation. A general upward coarsening trend in the lower part (62.5–97.3 m), from laminated bioturbated claystone (FA2 - Table 7) to bioturbated siltstone (FA3 - Table 7), is interpreted to be a regressive sequence going from an outer shelf depositional environment, to a middle to inner shelf setting. The change in lithology at 62.5 m depth in the core is interpreted to be the boundary between the Kolje Formation below and the Kolmule Formation above, and corresponds to horizon K2 (Marin et al., 2017; Grundvåg et al., 2017). Parallel simple stratified reflectors dominate S2 in the seismic data, suggesting little variations in lithology

Results and findings

across the study area. Reflector amplitude and continuity is reduced in the deeper basin, towards the south-west.

4.3.4 Sequence 3 – S3

Seismic description of S3

The remaining Lower Cretaceous succession in the seismic datasets, above surface K2, is collectively termed Sequence 3 (S3). The URU marks the upper boundary of S3. This unit is dominated by seismic facies SF3, SF4 and SF5 in dataset in ST0624, with rare occurrence of SF7 (Figure 4.3, Table 6). The seismic facies SF5 and SF6 dominate ST0811. Reflectors within S3 can be described as generally simple stratified parallel in configuration. Both amplitude strength and continuity vary between low and high, and are generally reduced in the deeper basin, towards the southwest.

Around salt diapirs the unit steeply dips, with internal reflectors terminating toplapping into the URU. High amplitude

reflectors in the lowest part of S3 disappear as they downlap onto K2 towards the southwest and into the basin. The TWTT thickness of the unit reaches its maximum in the south-western part of ST0624, where it is 1050 ms thick (Figure 4.10).

The depocenter in the study area for S3 is south of salt diapir D3, where the unit reaches 1000 ms time thickness from surface K2 to the URU. In the remaining main basin, northwards from the depocenter in the study area, the unit keeps around 600 ms time thickness.

Core description of S3

Sequence 3 occurs in the upper part of shallow stratigraphic core 7231/04-U-01 (Figure 4.7), between 37.2 m and 62.5 m depth. It is comprised of a dark grey claystone, with some siltstone intervals (FA3 - Table 7). Bioturbation occurs in the entire unit.

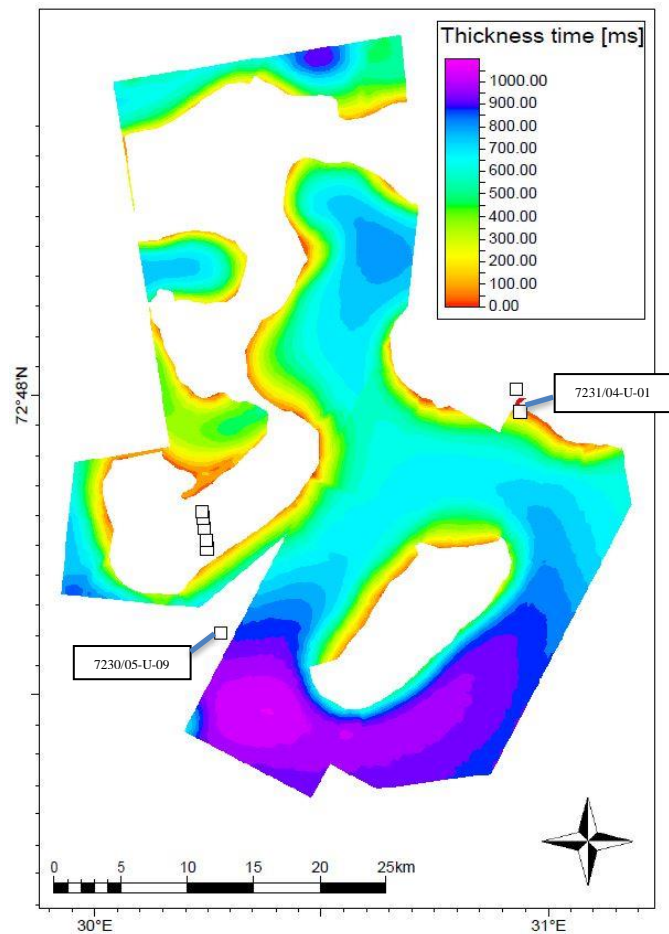


Figure 4.10 Time thickness map for Sequence 3 (S3), between K2 and the URU, in seismic dataset ST0624 and ST0811, in the central subbasin of the Nordkapp Basin.

Depositional environment of S3

The upper part of core 7231/04-U-01 corresponds to the lower part of the Kolmule Formation, and to S3 (Bugge et al., 2002; Grundvåg et al., 2017). The bioturbated dark grey claystone and siltstone suggest a middle shelf depositional environment. Parallel simple stratified reflectors dominate S3 in the seismic data, suggesting little variations in lithology across the study area, and wide-spread shelf conditions.

4.3.5 Younger Lower Cretaceous Sequence

In the regional study of Lower Cretaceous sequences by Marin *et al.* (2017), three additional younger sequences were described in the southwestern sub basin of the Nordkapp Basin, named S4–S6. Of these, none were defined in the study area. S5, however, is penetrated in a shallow core (7239/05-U-09) close southwest of the study area.

Description of S5 in core 7230/05-U-09

Shallow stratigraphic core 7230/05-U-09 correlates to Lower Cretaceous sequence S5 in Marin *et al.* (2017) (Appendix 1). This sequence is younger than the ones focused on in this study. The lithology of this core is sandier than that of the older ones described above. It comprises trough cross stratified fine grained sandstone (FA6 - Table 7), bioturbated fine grained sandstone and siltstone, low-angle trough cross laminated very fine grained sandstone, heavily bioturbated claystone with shell fragments (FA7 - Table 7) and laminated to bioturbated sandstone.

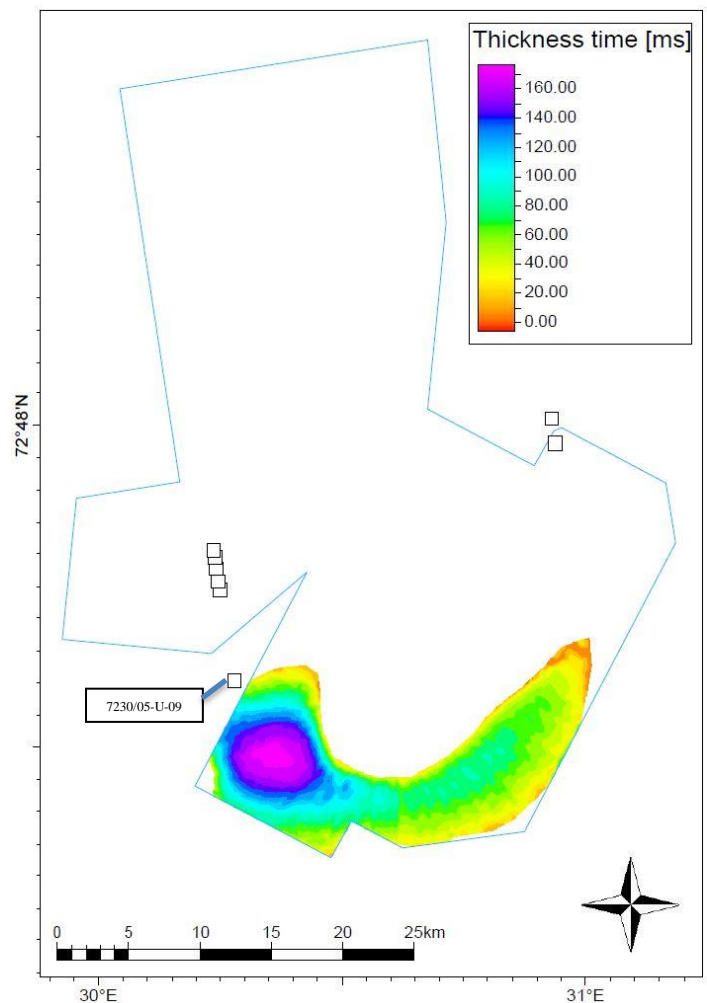


Figure 4.11. Time thickness map and subcrop of a high amplitude reflector interpreted in the upper S3. Time thickness between the URU and the reflector. Potentially the top of S3, and the extent of Upper Cretaceous units in the study area.

Interpretation of S5 in core 7230/05-U-09

The depositional environment of the 7230/05-U-09 core is interpreted to be part of a regressive unit, shallowing from inner shelf to shoreface deposits, and potentially lagoonal intervals towards the top (Bugge et al., 2002). It is part of the Kolmule Formation.

In the southwestern part of seismic dataset ST0624 a high amplitude reflector is found in the upper part of S3 as defined here (Figure 4.11). Based on the coring location of 7230/05-U-09 (Figure 4.11), and correlated to the seismic data, this reflector could mark the intra Kolmule Formation boundary between the Lower and Upper Cretaceous in the study area, and part of sequence S5 as defined in the cores (Bugge et al., 2002; Marin et al., 2017).

5 Discussion

5.1 Salt

5.1.1 Salt structures

The salt diapirs identified in the seismic data of the study area are some of the many in the Nordkapp Basin. 18 salt diapirs were identified in the central subbasin by Koyi *et al.* (1995), where they subcrop into the URU. Out of these, seven diapirs influence the study area succession, and are completely or partially located within the study area. All the diapirs in the study area are either single salt diapirs or parts of larger diapir systems, but no salt pillows are identified. Grimstad (2016) describes salt pillows in the central sub-basin of the Nordkapp Basin to be prominent at the western and southern boundaries of the basin – at the Nysleppen and Thor Iversen fault complexes, respectively. The orientation of the salt diapirs in the central basin is a W–E to SW–NE direction, following the basin margins (Grimstad, 2016; Koyi *et al.*, 1995).

Salt diapirs D2 and D4 are only partially in the study area, but influence the Lower Cretaceous succession by upturning it. The two diapirs are described by Grimstad (2016) as sub-circular in shape, with W–E orientations. The salt system type structures DS4a, DS4b, DS7 and DS8 in the study area are all individual structures at the URU subcrop, but merge into one larger salt body system at a shallower level. The main driving force for the location of where the original Permian salt deposits pierced the overburden, and the orientation of the diapirs, is by Koyi *et al.* (1995) attributed to faults in the basement below. Reactivation of these faults during regional extension would trigger diapirism in the area.

5.1.2 Salt activity during the Cretaceous Period

Of the successions in the seismic data used in this study, the Hekkingen Formation equivalent, sequence JS1 (Figure 4.5), and the lower most Lower Cretaceous sequence S1 (Figure 4.8), appears to distinctly decrease in time thickness towards salt diapirs. Sequence JS1 typically has a time thickness of 80 ms in the middle of rim synclines, but decreases above salt diapirs, to the point where the interpreted lower and upper boundary reflectors lie adjacent to each other (Figure 4.5), Lower Cretaceous sequence S1 typically holds a time thickness of 200 ms in the rim synclines of the study area, but decreases to 80–120 ms towards and above salt diapirs (Figure 4.8). Sequences S2–S3 are not observed to thin towards diapirs in the area studied. However these sequences do sub crop at the URU further away from salt structures than sequences JS1 and S1, and they may have thinned in areas that

Discussion

are now eroded (Figure 4.9, Figure 4.10). Both seismic units JS1 and S1–S3 seem to drape the salt diapirs in the area, as opposite to being cut off – however because of erosion the full units are no longer observable. The thinning of seismic units towards salt diapirs is attributed to the structure being a topographical high during deposition of the unit, or actively rising.

The timing of salt diapirs actively rising in the Nordkapp Basin during the Mesozoic, is still debated. Gabrielsen *et al.* (1990) suggested that the diapirs were actively rising during Triassic times, and later reactivated by tectonic episodes in the Late Jurassic to Early Cretaceous and Tertiary times. Koyi *et al.* (1995) suggest that after the Triassic rise, diapirs extruded as salt overhangs during Jurassic times, and were subsequently buried during Cretaceous times, although still rising. The diapirs continued rising during the Tertiary, although slower than the sedimentation rate, until they were uplifted and eroded during late Tertiary. Nilsen *et al.* (1995) suggest that diapir rise in the Nordkapp Basin is closely linked to episodes of regional extension and gravity gliding, during the Triassic, Late Jurassic and Late Cretaceous times. Compression during the middle Tertiary triggered a new episode of diapir rise. Bugge *et al.* (2002) suggest that the salt movements were active during the Early–Middle Triassic and Tertiary times, with only minor remobilization in-between the two events. Grimstad (2016) suggests that there was no salt movement in the Nordkapp Basin during Jurassic or Early Cretaceous, but successions from these times were later affected by reactivation during Late Cretaceous–Tertiary – though the exact timing is hard to identify due to erosion.

Based on the thinning of respectively units JS1 during the late Oxfordian–early Volgian, and S1 during latest Valanginian/earliest Hauterivian to early Barremian age, towards salt diapirs in the study area, the structures are suggested to be topographical highs during these times.

5.1.3 Salt influence on sediment routing

If the salt diapirs in the Nordkapp Basin were topographical highs during the Early Cretaceous, they would potentially have an influence on the routing of prograding sediments across the basin. To study this, the thickness of sedimentary units on the sides of salt diapirs are compared. A reduction in thickness on one side of a structure may indicate that the structure was an obstacle hindering the progradation of the unit.

The study area consists of one larger rim synclinal basin, and some smaller ones on the western and northern borders of the area, separated from the main basin by salt structures. Due to lack of available regional seismic data in this study, interpretation and correlation of

Discussion

key reflectors and units from the main basin to the distal rim synclinals were challenging. From the observed seismic data, none of the Lower Cretaceous units seem to vary significantly in time thickness between the main basin, and the distal rim synclinals. Time thickness variations of the units in the regional study by Marin *et al.* (2017) seem to be the result of depocenter migration and progradation of the units, and not to be affected by salt diapirs.

The uniform thickness of the Lower Cretaceous units in the Nordkapp Basin indicate that salt diapirs did not actively barrier during progradation and deposition of the units, which corresponds with observations by Nilsen *et al.* (1995).

5.2 Lower Cretaceous Sequences

The genetically related sedimentary sequences observed in the study area will be discussed in this chapter.

5.2.1 Sequence boundaries

All Lower Cretaceous key horizons identified (K0–K2) in this study correlate well to their correspondingly named horizons by Marin *et al.* (2017), representing flooding surfaces defining genetic stratigraphic sequences (S1–S3).

The K0 horizon is interpreted to be the formation boundary between the black shale Hekkingen Formation below, and the condensed carbonates of the Klippfisk Formation above. The formation boundary is seen in core 7231/01-U-01, where it represents a hiatus spanning the Early Volgian to Early Hauterivian (Bugge *et al.*, 2002).

The K1 horizon is interpreted to be a flooding surface, found in the seismic data as the top of large scale low angle clinoform reflectors in sequence S1. The regional flooding surface is also observed in core 7231/01-U-01, above the Klippfisk Formation, where a hiatus spanning the Late Hauterivian occurs (Bugge *et al.*, 2002). The horizon downlaps onto surface K0 where S1 wedges out towards the southwest.

Horizon K2 is interpreted to be a flooding surface and the formation boundary between the Kolje Formation below, and Kolmule Formation above, as described by Grundvåg *et al.* (2017). In the seismic dataset, the horizon is the boundary between S2 below, and S3 above. The horizon is a termination plane for reflectors in the lower part of S3, which downlap, terminating into it. K2 also occurs as a flooding surface in core 7231/04-U-01 (Bugge *et al.*, 2002; Grundvåg *et al.*, 2017).

5.2.2 Sequences

The stratigraphic sequences S1–S3 are found in the study area. These are part of the same Lower Cretaceous sequences that were investigated by Marin *et al.* (2017) across the southwestern Barents Shelf. In this study they were identified in the central sub-basin of the Nordkapp Basin.

S1

In the study area S1 contains parallel simple stratified reflectors of moderate to low amplitude strength, which wedge out towards the southwest, onto the BCU, in a low angle clinoform

Discussion

shape (Figure 4.3). As the sequence wedges out in study area, a distal part of a prograding sequence is inferred here. The main prograding direction is also suggested to be towards the southwest, the same as the direction the sequence wedges out in. The sequence thins towards salt diapirs in the study area, suggesting that the diapirs were active during the time of deposition, or local topographical highs. No local wedge shapes were observed in proximity to the salt diapirs however, suggesting that they were not local sediment sources for the sequence. The prograding sequence downlaps onto the BCU, near the K0 horizon, and the overlying Klippfisk Formation. The condensed carbonate Klippfisk Formation is considered to be part of the S1 Lower Cretaceous sequence.

Correlated to time thickness maps (Figure 4.8) and descriptions of the sequences by Marin *et al.* (2017), the S1 in the study area represents a distal bottomset part of the prograding sequence. The sequence prograded towards the southwest in the Nordkapp Basin, as well as on the Bjarmeland Platform, north of the study area.

Large scale clinofolds (130–400 m high), defined as shelf-margin size, are described to be found in sequence S1, but the interpreted maximum progradation area of these are northeast of the study area (Marin *et al.*, 2017). The age of S1 is suggested to be latest Valanginian/earliest Hauterivian to early Barremian, by Grundvåg *et al.* (2017).

Klippfisk Formation

A new Lower Cretaceous lithostratigraphic unit on the western Barents Shelf was introduced in 1998 (Smelror *et al.*, 1998). The unit had been described earlier by Århus (1991) and Århus *et al.* (1990) as a distinct condensed carbonate interval in cores from the Barents Shelf, and in outcrops on Kongsøya, eastern Svalbard (Smelror *et al.*, 1998). The Klippfisk Formation was observed in this study in core 7231/01-U-01. The interval between 59.9 m and 64.6 m comprises of a bioturbated greenish light gray and greenish light brown carbonate section, with nodular appearance. In the seismic data the unit was represented by a high amplitude peak reflector, directly overlying the trough reflector that was interpreted as top Hekkingen Formation. The reflector keeps a high amplitude throughout the entire study area, only interrupted by frequent faults, attributed to the BCU. The reflector dips slightly into the main rim synclinal basins, following the underlying K0 (Top Hekkingen) horizon.

This peak reflector was interpreted in the entire study area, except for areas where it was pulled up by salt diapirs and eroded by the URU. The reflector representing the Klippfisk

Discussion

Formation is also observed to be the termination plane for clinoform reflectors in S1, downlapping on it.

The unit in the core is dated to an early Hauterivian age by Bugge *et al.* (2002), with hiatus at the base of the unit spanning the early Volgian–early Hauterivian, and late Hauterivian at the top. Based on the thickness and fossil content, the depositional environment of the unit is suggested to be a condensed carbonate platform (FA4 - Table 7) (Bugge *et al.*, 2002; Smelror *et al.*, 1998).

S2

Sequence S2 in the study area contains parallel simple stratified reflectors, of moderate to high amplitude strength. The sequence runs parallel to the underlying S1, and BCU where the S1 is wedged out. In the study area the time thickness of S2 decreases towards the southwest (Figure 4.9), but does not completely wedge out in the area. No clinoform reflectors were observed in S2 in the study area, giving no indications for a shelf break location during the time of deposition. The sequence does not significantly thin towards salt diapirs in the study area, indicating that they were not topographical highs during the time.

The time thickness of S2 observed in the study area corresponds well to that presented by Marin *et al.* (2017). Marin *et al.* (2017) describes the maximum progradation of clinoforms in the sequence run through the study area, but no clinoform reflectors were observed in the seismic datasets available. If this is due to poor quality of the seismic datasets available during this study, or the maximum progradation area being interpolated from sidelying observations, is unsure.

Clinofoms in S2 in the Nordkapp Basin and the eastern Bjarmeland Platform are described as oblique, 40–60 m high and with high-gradient foresets (Marin *et al.*, 2017). The height is described as indicating sediments prograding in shallow water, exemplified as on continental shelves (Marin *et al.*, 2017; Helland-Hansen and Hampson, 2009).

Parts of sequence S2 were observed in cores 7231/01-U-01 and 7231/04-U-01, where it is represented by a coarsening upwards sequence from bioturbated and laminated claystone to bioturbated siltstone with shell fragments. This is interpreted to be deposited in an outer to middle to inner shelf setting, based on the occurring shell fragments and bioturbation indicating a marine setting. Sediment grain sizes indicating a relatively distal setting from the shore for the lower part of the unit, possible reflecting offshore. Bugge *et al.* (2002) also

Discussion

described these cores as parts of a southwesterly prograding sedimentary wedge unit, which correlates well to the observations done in this study.

The age of sequence S2 is suggested by Bugge *et al.* (2002) as Barremian to early Albian. Grundvåg *et al.* (2017) suggest the ages of latest Barremian–early late Aptian for the lower part of the sequence, and early Aptian–mid late Aptian for the upper part.

S3

The sequence S3 contains parallel simple stratified reflectors, of varying continuity and amplitude strength. The sequence dips towards the southwest in the study area, and thickens in the same direction. Near salt diapirs the sequence is pulled up, but does not show significant thinning. This may indicate that the diapirs were not topographical highs during the time S3 prograded over the study area.

Marin *et al.* (2017) describe the maximum progradation of clinoforms of the sequence to be located southwest of the study area, and to occur on the Bjarmeland and Finnmark platforms. The clinoforms in the vicinity of the Nordkapp Basin are described as large scale (500 m height), with low gradient foresets. The height indicates shelf margin clinoforms. In the study area no clinoform reflectors were observed in S3.

S3 occurs in core 7231/04-U-01, as a dark grey claystone, with some silty intervals, and minor bioturbation. A middle shelf depositional environment is suggested, and a relative deepening in setting compared to the underlying S2. Bugge *et al.* (2002) also describe this core section as a result of relative sea level rise, and as part of a new progradational unit. That this unit extends further to the southwest than the underlying unit is also noted by the authors. Grundvåg *et al.* (2017) suggest a latest Aptian/earliest Albian to early middle Albian age for S1.

5.2.3 Depocenter migration

The depocenter of a stratigraphic unit, where it is at its thickest, can in seismic data be observed on time thickness maps of the units. For the units S1–S3 observed in the study area, a stepwise southwesterly change in depocenter is seen. Sequence S1 in the study area is at its thickest in the north–northeast, at around 200 ms (Figure 4.8). S2 is thickest in the eastern part of the study area, at around 250 ms time thickness (Figure 4.9), whereas S3 is thickest in the southwestern part, reaching a height of 1050 ms (Figure 4.10).

Discussion

In the regional study of Lower Cretaceous prograding sequences by Marin *et al.* (2017), the same systematic displacement of the depocenters towards the southwest for S1–S3 in the Nordkapp Basin, is reported. To correlate the observations, the depocenter of S1 lies further to the northeast than the one observed in this study and reaches around 450 ms time thickness. The depocenter of S2 is marked slightly further east than in this study, and reaches around 750 ms time thickness. For S3, the depocenter is marked slightly south of the study area, and reaches approximately 1200 ms time thickness. The thickness of each sequence in the study area correlates well with the time thickness presented by Marin *et al.* (2017). Bugge *et al.* (2002) also noted that the overlying Lower Cretaceous units in the Nordkapp Basin extended further to the southwest than underlying units. Grundvåg *et al.* (2017) point out that the final shelf break for sequences S1–S3 developed south of the Nordkapp Basin.

5.2.4 Source Area

The step-wise migration of depocenter towards the southwest in the Lower Cretaceous sequences suggests the sediments accumulating from the northeast. As the study area is dominated by marine deposition, the source of the prograding sediments is likely not in the area. Indications of local sediment sources within the study area were also not found (wedges, fans). Of structural highs in the vicinity north–east of the Nordkapp Basin, the Fedynsky high (Figure 2.4) is a possible source area, uplifted during the Cretaceous (Kairanov *et al.*, 2018).

The source area for the sediments in the Lower Cretaceous successions in the Nordkapp Basin, is generally thought to be to the east and northeast of the Barents Shelf (Marin *et al.*, 2017; Grundvåg *et al.*, 2017; Kayukova and Suslova, 2015; Smelror *et al.*, 2009; Dimitriou, 2014). Uplift in the northern and northeastern parts of the Barents Shelf, during the Valanginian–Barremian, led to an increase in available terrigenous sediments (Smelror *et al.*, 2009). Kayukova and Suslova (2015) identified Lower Cretaceous prograding sequences on the eastern Barents Shelf, thought to be part of the same system identified by Marin *et al.* (2017) in the western part. The area close to Novaya Zemlya and Franz Josef Land, east–northeast of the Barents Shelf, is thought to be the source area for the sequences (Marin *et al.*, 2017; Kayukova and Suslova, 2015).

As no fan or wedge shapes were found near salt diapirs in the study area, they are not regarded as local sediment sources for the Lower Cretaceous sequences. Local submarine fans in the Hammerfest Basin, fed from the Finnmark Platform and Loppa High, have earlier been identified by Marin *et al.* (2017). Indications of the main source area for the sequences being

the Fedynsky high or the Novaya Zemlya and Franz Josef Land area were not found within the study area.

5.3 Implications for paleogeographic development

Based on the observations and interpretations done in the 3D seismic data of the study area, and the correlation to the shallow stratigraphic cores, as well as results from earlier studies (Marin et al., 2017; Bugge et al., 2002), five paleogeographic maps for Early Cretaceous are presented (Figure 5.1).

During the Late Oxfordian–Early Volgian (sequence JS1) the central subbasin of the Nordkapp Basin was part of a basin with restricted circulation, leading to anoxic–dysoxic conditions (Bugge et al., 2002; Smelror et al., 2009; Worsley, 2008) (Figure 5.1A). The finely laminated black shales of the Hekkingen Formation (FA1 - Table 7) were deposited during this time. The thickness variation of the sequence (Figure 4.5), thickening in the basins and narrowing towards salt diapirs, indicate that the diapirs were topographical highs or actively rising during the time.

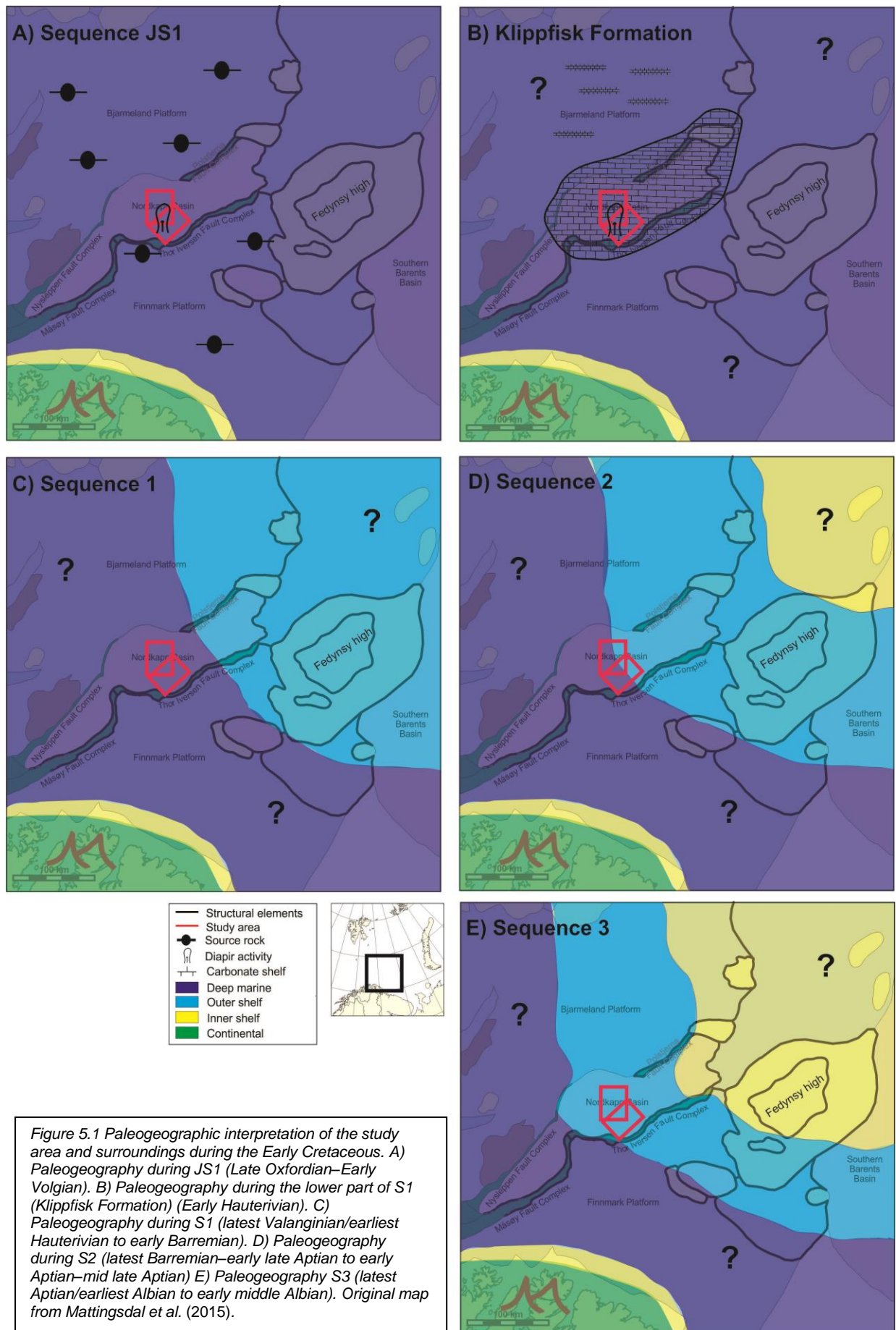
In the early Hauterivian a carbonate shelf (FA4 - Table 7) had formed in the basin, and the Klippfisk Formation was deposited across large parts of the shelf, particularly on platforms and highs (Bugge et al., 2002; Århus, 1991) (Figure 5.1B). An outer shelf setting carbonate platform is inferred for the study area. The Klippfisk Formation is recognized as the lowermost part of the Lower Cretaceous sequence 1 (S1).

During the latest Valanginian/earliest Hauterivian to early Barremian (S1) (from Grundvåg *et al.* (2017)) large sedimentary units were prograding across the eastern Barents Shelf. In this part of the Barents Shelf, these were sourced from Novaya Zemlya and Franz Josef Land and the prograding sequences reached the Nordkapp Basin in this time (Marin et al., 2017; Dimitriou, 2014; Kayukova and Suslova, 2015). In the study area, distal parts of the prograding unit S1 are inferred in an outer shelf setting, in the central basin of the Nordkapp Basin (Figure 5.1C). The thinning of this unit towards salt diapirs may indicate that they were active during this time.

Throughout the rest of the Early Cretaceous the sedimentary units kept prograding towards the southwest, causing a generally regressive trend in deposition in the study area (Bugge et

Discussion

al., 2002). The unit S2 of latest Barremian–early late Aptian to Early Aptian–mid late Aptian age (from Grundvåg *et al.* (2017)) shows a regressive trend from an outer to inner shelf environment, close to the study area (FA2, 3, 5 - Table 7) (Figure 5.1D). The overlying S3 of latest Aptian/earliest Albian to early middle Albian age, is interpreted to be deposited in a middle shelf setting in the study area (Figure 5.1E). Even younger units documented in core 7230/05-U-09 from the vicinity of the study area, show a shallow shelf to shoreface depositional environment (FA5–7, Table 7), from the Middle Albian–Lower Cenomanian Kolmule Formation (Bugge *et al.*, 2002). This suggests a regional regressive trend.



Discussion

6 Summary and conclusion

This study used two 3D seismic datasets, ST0624 and ST0811, to investigate the Lower Cretaceous succession, and salt diapirs, in the central sub-basin of the Nordkapp Basin. In the study area seven salt diapirs were identified which affect the Lower Cretaceous succession. The salt was originally deposited during the Late Carboniferous, and diapirism peaked in activity during the Early–Middle Triassic (Nilsen et al., 1995; Gabrielsen et al., 1990). Later reactivation of the salt diapirs took place during the Late Jurassic, Cretaceous and Tertiary. The timing of the Jurassic and Cretaceous reactivation is uncertain (Gabrielsen et al., 1990; Nilsen et al., 1995; Koyi et al., 1995). Observed thinning of sedimentary units towards salt diapir flanks in seismic data from the study area suggests diapir reactivation during the Late Jurassic and during the deposition of Lower Cretaceous sequence S1 (latest Valanginian/earliest Hauterivian to early Barremian age, Grundvåg *et al.* (2017)). Later reactivation during the Late Cretaceous and/or Tertiary made the diapirs pierce the Cretaceous succession, where they subcrop into Quaternary overburden today.

Three Lower Cretaceous sequences (S1–S3) were identified in the seismic data of the study area, and correlated to shallow stratigraphic cores. In the present seismic data the sequences consist of plane parallel reflectors dipping towards the southwest. Near salt diapirs the Cretaceous sequences are pulled up, and erosionally truncated by the Upper Regional Unconformity (URU). Sequence 1 was found to thin towards diapir flanks, indicating activity in the diapirs during the time of deposition.

The sequence S1 thins greatly towards the southwest in the study area, downlapping and wedging out onto the surface K1 (Top Hekkingen Formation equivalent). Sequence S2 has a relatively consistent time thickness in the study area, with a maximum thickness in the eastern part. Sequence S3 thickens towards the SW in the study area. The depocenter of the Lower Cretaceous succession (maximum thickness) thus systematically displaces from the NE towards SW. This is interpreted to be the result of prograding sedimentary units building out on the Barents Shelf during the Early Cretaceous. The source of the sediments is assumed to be in the vicinity of Novaya Zemlya and Franz Josef Land, in the east–northeastern part of the Barents Shelf, in accordance with other studies.

The shallow stratigraphic cores 7231/01-U-01, 7231/04-U-01 and 7230/05-U-09 were used in this study to get insight to the depositional environments of the Lower Cretaceous succession in the Nordkapp Basin. The cores show a general regressive trend, from outer to inner shelf

Summary and conclusion

and shoreface depositional environments. Correlated to the trends of prograding sedimentary sequences in the seismic data, and low angle clinoform reflectors observed in S1, this indicates a regional regressive trend in the Lower Cretaceous. Core 7231/01-U-01 also penetrated the Upper Jurassic Hekkingen Formation consisting of finely laminated black shale, which is the dominant petroleum system source rock on the Barents Shelf (Langrock and Stein, 2004). The same core also penetrated the Klippfisk Formation, a carbonate unit thought to have been deposited on a carbonate shelf in the study area, representing the lowest part of sequence S1 (Bugge et al., 2002).

This study may contribute to a better understanding of the Lower Cretaceous succession and paleogeography on the Norwegian Barents Shelf, although further studies and investigations are recommended.

References

- Ahlborn, M., and Stemmerik, L., 2015, Depositional evolution of the Upper Carboniferous – Lower Permian Wordiekammen carbonate platform, Nordfjorden High, central Spitsbergen, Arctic Norway: *Norwegian Journal of Geology*, v. 95, p. 91–126, doi: 10.17850/njg95-1-03.
- Andreassen, K., 2009, *Marine Geophysics Lecture Notes for Geo-3123*, University of Tromsø:.
- Brown, A.R., 2011, *Interpretation of Three-Dimensional Seismic Data* (S. E. Laubach & V. Grechka, Eds.): Tulsa, Oklahoma, Society of Exploration Geophysicists and American Association of Petroleum Geologists, doi: 10.1190/1.9781560802884.
- Bugge, T., Elvebakk, G., Fanavoll, S., Mangerud, G., Smelror, M., Weiss, H.M., Gjelberg, J., Kristensen, S.E., and Nilsen, K., 2002, Shallow stratigraphic drilling applied in hydrocarbon exploration of the Nordkapp Basin, Barents Sea: *Marine and Petroleum Geology*, v. 19, p. 13–37, doi: 10.1016/S0264-8172(01)00051-4.
- Dimitriou, M., 2014, Master Thesis: Lower Cretaceous Prograding Units in the eastern part of the SW Barents Sea: UiO, <https://www.duo.uio.no/handle/10852/42303>.
- Doré, A.G., 1995, Barents Sea Geology, Petroleum Resources and Commercial Potential: *ARCTIC*, v. 48, p. 207–221, doi: 10.14430/arctic1243.
- Faleide, J.I., Bjørlykke, K., and Gabrielsen, R.H., 2015, Geology of the Norwegian Continental Shelf, *in* *Petroleum Geoscience*, Berlin, Heidelberg, Springer Berlin Heidelberg, p. 603–637, doi: 10.1007/978-3-642-34132-8_25.
- Faleide, J.I., Gudlaugsson, S.T., and Jacquart, G., 1984, Evolution of the western Barents Sea: *Marine and Petroleum Geology*, v. 1, p. 123–150, doi: 10.1016/0264-8172(84)90082-5.
- Faleide, J.I., Tsikalas, F., Breivik, A.J., Mjelde, R., Ritzmann, O., Engen, Ø., Wilson, J., and Eldholm, O., 2008, Structure and evolution of the continental margin off Norway and the Barents Sea: *Episodes*, v. 31, p. 82–91, doi: 10.1016/j.strusafe.2006.11.005.
- Faleide, J.I., Vågnes, E., and Gudlaugsson, S.T., 1993, Late Mesozoic-Cenozoic evolution of the south-western Barents Sea in a regional rift-shear tectonic setting: *Marine and*

Summary and conclusion

Petroleum Geology, v. 10, p. 186–214, doi: 10.1016/0264-8172(93)90104-Z.

Fossen, H., 2010, Structural Geology, *in* Structural Geology, Cambridge, Cambridge University Press, p. 371–393, doi: 10.1017/CBO9780511777806.

Gabrielsen, R.H., Færseth, R.B., Jensen, L.N., Kalheim, J.E., and Riis, F., 1990, NPD-Bulletin No 6 Structural Elements of the Norwegian continental shelf: Norwegian Petroleum Directorate Bulletin, v. 6, p. 1–47.

Galloway, W.E., 1989, Genetic stratigraphic sequences in basin analysis I: architecture and genesis of flooding-surface bounded depositional units: American Association of Petroleum Geologists Bulletin, v. 73, p. 125–142, doi: 10.1306/703C9AF5-1707-11D7-8645000102C1865D.

Gernigon, L., Brönnert, M., Roberts, D., Olesen, O., Nasuti, A., and Yamasaki, T., 2014, Crustal and basin evolution of the southwestern Barents Sea: From Caledonian orogeny to continental breakup: Tectonics, v. 33, p. 347–373, doi: 10.1002/2013TC003439.

Giles, K.A., and Lawton, T.F., 2002, Halokinetic sequence stratigraphy adjacent to the El Papalote diapir, northeastern Mexico: AAPG Bulletin, v. 86, p. 823–840, doi: 10.1306/61EEDBAC-173E-11D7-8645000102C1865D.

Giles, K.A., and Rowan, M.G., 2012, Concepts in halokinetic-sequence deformation and stratigraphy: Geological Society, London, Special Publications, v. 363, p. 7–31, doi: 10.1144/SP363.2.

Glørstad-Clark, E., Faleide, J.I., Lundschie, B.A., and Nystuen, J.P., 2010, Triassic seismic sequence stratigraphy and paleogeography of the western Barents Sea area: Marine and Petroleum Geology, v. 27, p. 1448–1475, doi: 10.1016/j.marpetgeo.2010.02.008.

Grimstad, S., 2016, Master Thesis in Geoscience: Salt tectonics in the central and northeastern Nordkapp Basin, Barents Sea: University of Oslo, 0-117 p.

Grundvåg, S.-A., Marin, D., Kairanov, B., Sliwinska, K.K., Nøhr-Hansen, H., Jelbye, M.E., Escalona, A., and Olaussen, S., 2017, The Lower Cretaceous succession of the northwestern Barents Shelf: Onshore and offshore correlations: Marine and Petroleum Geology journal, v. 86, p. 834–857, doi: 10.1016/j.marpetgeo.2017.06.036.

Summary and conclusion

- Gudlaugsson, S.T., Faleide, J.I., Johansen, S.E., and Breivik, A.J., 1998, Late Palaeozoic structural development of the South-western Barents Sea: Marine and Petroleum Geology, v. 15, p. 73–102, doi: 10.1016/S0264-8172(97)00048-2.
- Halland, E.K., Bjørnstad, A., Gjeldvik, I.T., Bjørheim, M., Magnus, C., Meling, I.M., Mujezinović, J., Riis, F., Rød, R.S., Pham, V.T.H., and Tappel, I., 2011, CO2 Storage Atlas: The Barents Sea, *in* Halland, E.K., Bjørnstad, A., Gjeldvik, I.T., Bjørnheim, M., Magnus, C., Meling, I.M., Mujezinović, J., Riis, F., Rød, R.S., Pham, V.T.H., and Tappel, I. eds., CO2 Storage Atlas Norwegian Sea, p. 107–145.
- Helland-Hansen, W., and Hampson, G.J., 2009, Trajectory analysis: Concepts and applications: Basin Research, v. 21, p. 454–483, doi: 10.1111/j.1365-2117.2009.00425.x.
- Henriksen, E., Ryseth, A.E., Larssen, G.B., Heide, T., Ronning, K., Sollid, K., and Stoupakova, A. V., 2011, Chapter 10 Tectonostratigraphy of the greater Barents Sea: implications for petroleum systems: Geological Society, London, Memoirs, v. 35, p. 163–195, doi: 10.1144/M35.10.
- Jackson, M.P.A., and Hudec, M.R., 2017, Salt Tectonics: Cambridge, Cambridge University Press, 498 p., doi: 10.1017/9781139003988.
- Jones, I.F., and Davison, I., 2014, Seismic imaging in and around salt bodies: Interpretation, v. 2, p. SL1–SL20, doi: 10.1190/INT-2014-0033.1.
- Kairanov, B., Escalona, A., Mordasova, A., Śliwińska, K.K., and Suslova, A.A., 2018, Lower Cretaceous tectonostratigraphic evolution of the northcentral Barents Sea: Journal of Geodynamics, doi: 10.1016/j.jog.2018.02.009.
- Kayukova, A. V., and Suslova, A.A., 2015, A seismostratigraphic analysis of the lower cretaceous deposits of the Barents sea to reveal petroleum perspectives: Moscow University Geology Bulletin, v. 70, p. 177–182, doi: 10.3103/S0145875215020040.
- Koyi, H., Talbot, C.J., and Tørudbakken, B.O., 1993, Salt diapirs of the southwest Nordkapp Basin: analogue modelling: Tectonophysics, v. 228, p. 167–187, doi: 10.1016/0040-1951(93)90339-L.
- Koyi, H., Talbot, C.J., and Tørudbakken, B.O., 1995, Salt Tectonics in the Northeastern

Summary and conclusion

Nordkapp Basin, Southwestern Barents Sea: Aapg Memoir, p. 437–447.

Langrock, U., and Stein, R., 2004, Origin of marine petroleum source rocks from the Late Jurassic to Early Cretaceous Norwegian Greenland Seaway-evidence for stagnation and upwelling: *Marine and Petroleum Geology*, v. 21, p. 157–176, doi: 10.1016/j.marpetgeo.2003.11.011.

Lundschieen, B.A., Høy, T., and Mørk, A., 2014, Triassic hydrocarbon potential in the northern Barents Sea; integrating Svalbard and stratigraphic core data: *Norwegian Petroleum Directorate Bulletin*, v. 11, p. 3–20.

Marin, D., Escalona, A., Śliwińska, K.K., Nøhr-Hansen, H., and Mordasova, A., 2017, Sequence stratigraphy and lateral variability of Lower Cretaceous clinofolds in the southwestern Barents Sea: *AAPG Bulletin*, v. 101, p. 1487–1517, doi: 10.1306/10241616010.

Mattingsdal, R., Høy, T., Simonstad, E., and Brekke, H., 2015, An updated map of structural elements in the southern Barents Sea Abstract: *Norwegian Petroleum Directorate poster*, p. 9488.

Mitchum Jr., R.M., Vail, P.R., and Sangree, J.B., 1977, *Seismic Stratigraphy and Global Changes of Sea Level, Part 6: Stratigraphic Interpretation of Seismic Reflection Patterns in Depositional Sequences: Seismic Stratigraphy — applications to hydrocarbon exploration*, v. 165, p. 117–134, doi: 10.1038/272400a0.

Nichols, G., 2009, *Sedimentology and Stratigraphy*: John Wiley & Sons.

Nilsen, K.T., Vendeville, B.C., and Johansen, J.-T., 1995, Influence of Regional Tectonics and Halokinesis in the Nordkapp Basin, Barents Sea, *in* Jackson, D.G. and Snelson, S. eds., *Salt tectonics: a global perspective*: AAPG Memoir 65, p. 413–436.

NPD, 2016, Barents Sea - Upper Jurassic to Lower Cretaceous plays: 13.04.2016, <http://www.npd.no/en/Topics/Geology/Geological-plays/Barents-Sea/Upper-Jurassic-to-Lower-Cretaceous/> (accessed November 2017).

NPD, 2017, NPD FactPages:., <http://factpages.npd.no/factpages/>.

Polteau, S., Hendriks, B.W.H., Planke, S., Ganerød, M., Corfu, F., Faleide, J.I., Midtkandal,

Summary and conclusion

- I., Svensen, H.S., and Myklebust, R., 2016, The Early Cretaceous Barents Sea Sill Complex: Distribution, $^{40}\text{Ar}/^{39}\text{Ar}$ geochronology, and implications for carbon gas formation: *Palaeogeography, Palaeoclimatology, Palaeoecology*, v. 441, p. 83–95, doi: 10.1016/j.palaeo.2015.07.007.
- Riis, F., Lundschieen, B.A., Høy, T., Mørk, A., and Mørk, M.B.E., 2008, Evolution of the Triassic shelf in the northern Barents Sea region: *Polar Research*, v. 27, p. 318–338, doi: 10.1111/j.1751-8369.2008.00086.x.
- Rise, L., and Sættem, J., 1994, Shallow stratigraphic wireline coring in bedrock offshore Norway: *Scientific Drilling*, p. 243–257.
- Rojo, L.A., Escalona, A., and Schulte, L., 2016, The use of seismic attributes to enhance imaging of salt structures in the Barents Sea: *First Break*, v. 34, p. 49–57, doi: 10.3997/1365-2397.2016014.
- Ryseth, A.E., Augustson, J.H., Charnock, M., Haugerud, O., Knutsen, S.M., Midbøe, P.S., Opsal, J.G., and Sundsbø, G., 2003, Cenozoic stratigraphy and evolution of the Sørvestsnaget Basin, southwestern Barents Sea: *Norsk Geologisk Tidsskrift*, v. 83, p. 107–130.
- Sheriff, R.E., 1985, Aspects of seismic resolution: *AAPG Memoir*, v. 39, p. 1–10.
- Sheriff, R.E., 2002, *Encyclopedic Dictionary of Applied Geophysics*: Tulsa, Society of Exploration Geophysicists, doi: 10.1190/1.9781560802969.
- SINTEF, 2009, *Shallow Stratigraphic Drilling projects 1982-1993*..
- Smelror, M., Mørk, A., Monteil, E., Rutledge, D., and Leereveld, H., 1998, The Klippfisk formation - a new lithostratigraphic unit of Lower Cretaceous platform carbonates on the Western Barents Shelf: *Polar Research*, v. 17, p. 181–202, doi: 10.1111/j.1751-8369.1998.tb00271.x.
- Smelror, M., Petrov, O., Larssen, G.B., and Werner, S., 2009, *Atlas: Geological History of the Barents Sea* (M. Smelror, O. V Petrov, G. B. Larssen, & S. Werner, Eds.): Trondheim, Geological Survey of Norway.
- Trusheim, F., 1960, Mechanism of Salt Migration in Northern Germany: *AAPG Bulletin*, v.

Summary and conclusion

44, p. 1519–1540, doi: 10.1306/0BDA61CA-16BD-11D7-8645000102C1865D.

Worsley, D., 2008, The post-Caledonian development of Svalbard and the western Barents Sea: *Polar Research*, v. 27, p. 298–317, doi: 10.1111/j.1751-8369.2008.00085.x.

Århus, N., 1991, The transition from deposition of condensed carbonates to dark claystones in the Lower Cretaceous succession of the southwestern Barents Sea: *Norsk Geologisk Tidsskrift*, v. 71, p. 259–263.

Århus, N., Kelly, S.R.A., Collins, J.S.H., and Sandy, M.R., 1990, Systematic palaeontology and biostratigraphy of two Early Cretaceous condensed sections from the Barents Sea: *Polar Research*, v. 8, p. 165–194, doi: 10.1111/j.1751-8369.1990.tb00383.x.

Appendix 1 Log of core 7230/05-U-09

7230/05-U-09 1:250

